Characterization of Commercial Carbon fiber from Standard PAN Precursors and Low-Cost Carbon Fiber from Textile PAN based Precursors

A Thesis Presented for the
Master of Science
Degree
The University of Tennessee, Knoxville

Joshua David Crabtree
May 2019

DEDICATION

I dedicate this thesis to my mom, Robin, dad, David, and brother, Ethan, for their unending love, support, prayers, and encouragement during this program. I would also like to dedicate this to all my friends that I worked with at the Carbon Fiber Technology Facility, especially Rick and Tonia, for their help and guidance. I dedicate this work to all my close friends and church family that have stuck with me, prayed for me, and shared encouraging words through this process which have been a blessing. Finally, and most importantly, I dedicate this work to my Lord and Savior Jesus Christ for being the rock upon which I stand!

ACKNOWLEDGEMENTS

The work presented herein would not have been possible without the consistent guidance and wisdom from my principal adviser, Dr. Dayakar Penumadu who patiently helped me understand, grasp concepts, and improve my technical writing. My wholehearted appreciation also goes to the distinguished members of my Committee, Dr. Uday Vaidya and Dr. David Harper for reviewing of this thesis. I want to thank Dr. Stephen Young for all his help and guidance through my course of study and Dr. Matt Kant for helping me understand certain concepts needed in this work. In addition, I would like to express gratitude to Ken Thomas for always being there to talk and keep me laughing. Finally, I would like to acknowledge all of Dr. Penumadu's group members (graduate and undergraduate) for listening to me discuss (complain) about my work. It has been a joy working with you and I couldn't have made it without y'all!

ABSTRACT

There is tremendous need to integrate carbon fiber composites for light-weighting in the transportation sector, especially for automotive composites and in energy generation space associated with wind turbine manufacturing. Tensile properties of carbon fibers are fundamental to designing fiber reinforced polymers and carbon/carbon composites. Carbon fiber suppliers typically follow general guidelines prescribed in the relevant standards (ASTM D4018) to prepare resin reinforced carbon fiber tows for determining the tensile properties. In this study, the effect of manufacturing process associated with carbon fiber tows was evaluated using two methods involving manual tensioned strands or using automated spool method. Important effects associated with fiber spacing, cross-sectional morphology of the infused tows are reported in this study. Single fiber mechanical properties are determined to obtain relationship from multiple length scales and the role of interfacial behavior between the carbon fiber and resin system using single fiber fragmentation. These results, for the first time, revealed important relationships between single fiber, interface, and infused tow based mechanical properties. A new concept for deformation response of infused tows, limit stress, demonstrated a connection in the nonlinearity nature of tensile modulus seen for carbon fibers in single fiber state and in tow format. Limit stress showed good representation of the relative role of relationships (interfacial behavior, crack propagation, and stress transfer) from limit stress to failure stress.

Three low-cost precursors, oxidized PAN, and carbon fiber, from the Carbon Fiber Technology Facility with differences in spin finish and/or tenacity are studied in detail through various stages of oxidative stabilization and carbonization to develop improved understanding of the precursor properties and final textile PAN based carbon fiber properties. A systematic

approach consisting of DSC, TGA, FT-IR, XRD, single fiber testing, and infused tow testing were considered in evaluating the process-structure-tensile property relationship for the three precursors. The results identified the role of spin finish and tenacity on the performance of low-cost carbon fiber. This part of the research provides an important conclusion that the carbon fiber manufacturing process using textile PAN precursors is industrially robust and is not strongly dependent on precursor tenacity or surface finish.

TABLE OF CONTENTS

Introduction 1

Chapter 1 Multiscale Investigation of Carbon Fiber Properties using Various Techniques 3

Abstract 4

1.1 Introduction 5

1.2 Materials and Methods 7

1.2.1 Materials 7

1.2.2 Imaging 8

1.2.3 Mechanical Testing 8

1.3 Results and Discussion 10

1.3.1 Single Fiber Analysis 10

1.3.2 Cross-sectional area comparison using Density/Linear Density and SEM 11

1.3.3 Infused tow analysis 11

1.4 Conclusions 16

1.5 Appendix 18

Chapter 2 Thermal-Mechanical Analysis of Textile PAN and the Structure-Property-Process Relationship 30

Abstract 31

2.1 Introduction 32

2.2 Materials and Methods 33

2.2.1 Materials 33

2.2.2 Characterizations 34

2.3 Results and Discussion 36
2.3.1 FT-IR Spectra Analysis 36
2.3.2 X-Ray Diffraction Microstructure 37
2.3.3 Thermal Characterization 38
2.3.4 Mechanical Behavior of Textile Carbon Fiber 40
2.4 Conclusions 43
2.5 Appendix 45
Conclusion 55
References 56
Vita 67

LIST OF TABLES

Table 1 Single fiber fragmentation data..... 28

Table 2 Cross-sectional area calculations based on linear density/density and SEM average diameter..... 28

Table 3 Comparison of mechanical properties of single filament, manual, automated, and dry methods..... 29

Table 4 X-ray diffraction peak locations, full width half max (FWHM), d-spacing, and stack height..... 53

Table 5 DSC thermal characterization analysis data 53

Table 6 Single filament Weibull strength and shape parameters..... 53

Table 7 Average single filament mechanical results using normal distribution..... 54

Table 8 Infused tow mechanical properties 54

LIST OF FIGURES

Figure 1 - Example setup of impregnation process using the manual and automated methods described within the ASTM D4018. 18

Figure 2 - Single fiber fragmentation mold demonstrating pre-tensioning and impregnation of the single carbon fiber..... 19

Figure 3 - Example tabbed single filament carbon fiber and impregnated carbon fiber tows..... 19

Figure 4 - Single filament Weibull statistical distribution demonstrating..... 20

Figure 5 - Optical micrograph showing fiber fractures exhibiting crack propagation and interfacial mechanical failure along the fiber. 20

Figure 6 - SEM micrograph showing cross-section of commercial grade 24k carbon fiber 21

Figure 7 - Distribution of Failure Stress and Modulus for flat and round tows, demonstrating increased failure stress of the round (manual) tow preparation against the flat (automated) tow preparation, and the statistically indistinguishable difference in modulus. 22

Figure 8 - Example mechanical response for single flat tow test, demonstrating a modulus drop associated with cracking and delamination of fiber and resin during tensile deformation... 22

Figure 9 - The composite stress/strain response for (A) flat, (B) round, and (C) unisized round impregnated fiber tows relative to all the raw data. 23

Figure 10 - Composite stress/strain and modulus/strain response for samples examined here, noting that the single fiber modulus continues to increase with strain magnitude, while tow moduli begin to decrease as sample damage accumulates..... 24

Figure 11 – Graphical demonstration of limit stress for (A) flat, (B) round, and (C) unisized round impregnated fiber tows. The decrease in the limit stress for the unsized round and flat tow relative to the round tow indicates the increase inter-fiber effects from the manufacturing technique used. 25
Figure 12 - Stress strain data with normalized acoustic energy layover demonstrating fiber and matrix fracturing for a) sized round infused tow b) sized flat infused tow c) unsized round infused tow and d) dry uninfused tow..... 26
Figure 13 - Microscopy showing example cross sections of the infused flat and round tow demonstrating resin voids, fiber packing, and overall structure. 27
Figure 14 - Potential variation in tensioning of the fibers that could occur during impregnation process..... 28
Figure 15 - SEM comparing the a) kidney bean cross-section shape of the textile carbon fiber b) circular cross-section of commercial carbon fiber..... 45
Figure 16 - Example tensile testing setup of a) single fiber testing using the Nano UTM and b) infused tow testing using the MTS test system..... 45
Figure 17 - Example procedure of a) fiber tow infusion b) rack attachment to keep taut c) final tabbed strand 46
Figure 18 - FT-IR spectra of textile PAN precursors A, B, and C before oxidation showing starting surface functional groups. 46
Figure 19 - FT-IR spectra of the textile PAN fibers A, B, and C after oxidation demonstrating surface functional groups increase/decrease from the precursor. 47

Figure 20 - Schematic illustration of the PAN structural levels: a) macromolecule helical structure; b) macromolecular orientation; c) fibril.Note: Reprinted from Violeta Florina Anghelina et al. Structural analysis of PAN fiber by X-ray diffraction, Journal of Science and Arts 1(12) (2010) 89-94 [50]..... 47
Figure 21 - X-ray diffraction patterns for a) commercial PAN pure and oxidized b) textile PAN pure and oxidized Note a) is a reprint from R. B. Mathur “Structure of thermally stabilized PAN fibers”, Carbon 29(7) (1991) 1059-1061 [49]..... 48
Figure 22 - Comparison of x-ray diffraction pattern for the 2θ a) fiber A, B, and C b) fiber A, B, and C OPF; and orientation comparison of c) fiber A, B, and C precursor and d) fiber A, B, and C OPF..... 49
Figure 23 - TGA thermogram (nitrogen atmosphere) of the three precursors and oxidized PAN fibers showing mass loss prior to carbonization..... 50
Figure 24 - DSC analysis comparing a fast and slow heating rate and the effect the environment has on the thermal analysis using nitrogen (inert) atmosphere and air atmosphere. 50
Figure 25 - DSC thermogram of the precursor for fiber A, B, and C showing similar peak temperatures and measured enthalpies..... 51
Figure 26 - DSC thermogram of the oxidized PAN fiber A, B, and C demonstrating similar enthalpy values for each fiber and a peak at `100 °C indicating moisture evaporation. 51
Figure 27 - Weibull distribution of single filament data for fiber A, B, and C showing consistent strength and scale parameters. The low scale parameters (1.66, 1.89, 2.08) demonstrate high strength variation. 52

INTRODUCTION

Carbon fiber reinforced composites have a variety of structural and functional applications. The superior mechanical properties (high strength and modulus) of carbon fiber is very appealing to a variety of markets such as aerospace and automotive. Due to the requirements of passenger safety for these markets, there is potentially high risk in using materials that are not well-understood. Thus, an understanding of material behavior on both a micro and macro scale is critical. Previous work has led to the establishment of standardized testing procedures for carbon fiber tows, such as the ASTM D4018 standard. Within this standard, there are various acceptable manufacturing protocols for infused carbon fiber tows that could lead to potentially widely varying tensile properties that are often reported by the carbon fiber manufacturers. For example, the method of infusing a tow of carbon fiber can be either manual or automated leading to widely varying results in tensile properties due to fundamental differences in the microstructure and relative tautness of single filaments within an infused and cured composite tow. The manufacturing process of infused tows could have a profound effect on the mechanical properties and thus needs to be further analyzed. It is well-known that an infused tow is one of the simplest cases of a composite. However, it is not well-known how infused tow properties translate from single fiber properties. Chapter 1 focuses on the relationship between single fiber and tow properties by studying how manufacturing methods allowed under the ASTM D4018 standard lead to variations in such properties.

The high cost of carbon fiber has often hindered adoption by high volume markets such as that of the automotive industry. In response, low-cost carbon fiber or textile carbon fiber

precursors are under development. For example, the polyacrylonitrile (PAN) that is used in low-cost carbon fiber at the Carbon Fiber Technology Facility (CFTF) is textile-based and is typically used in carpet manufacturing. Using textile-based PAN can lead to challenges that might not be encountered with traditional commercial PAN. To develop a better understanding of this textile fiber a systematic study of the conversion process relating to the thermal-mechanical properties at various stages within the conversion was undertaken. Chapter 2 focuses on the effect of spin finish and/or tenacity on the overall carbon fiber properties.

CHAPTER 1
MULTISCALE INVESTIGATION OF CARBON FIBER PROPERTIES USING VARIOUS TECHNIQUES

This chapter is a slightly revised version of a paper with the same title submitted for the Journal of Composites Science and Technology in 2019 by Joshua D. Crabtree, Matt Kant Dayakar Penumadu, and Stephen Young.

My primary contributions to this paper include: (i) development of the problem into a work, (ii) identification of the study areas, (iii) gathering and reviewing of literature, (iv) sampling, processing, and analyzing data from various methods of testing, (v) pulling various contributions into a single paper, (v) most of the writing.

Abstract

In the work presented here, mechanical properties of a commercial 24k carbon fiber were obtained by single filament, single fiber fragmentation, and tow bundle testing in flat and round geometrical formulations. The impregnated tows were found to have a tensile strength of 5,200 MPa for round geometry and 4,900 MPa for flat geometry. The relatively small variation in strength suggests that despite a significant alteration of sample geometry (and therefore fiber packing), variations in fiber load sharing do not significantly affect the mechanical performance of UD impregnated tows with adequate interfacial shear strength between fiber and resin. Single fiber fragmentation testing was performed to study the interfacial shear strength (IFSS) between the fiber and resin. The results indicate a 22 MPa IFSS with a fracture length of 438 μm. Single fiber tensile tests reveal a failure stress of 4,400 MPa, about 20% less than the tow tests. Limit stress is a new approach to define the strength of carbon fiber tows based on single fiber elastic behavior being non-linear with tensile strain. This technique yielded a stress comparable to the failure stress of single fiber demonstrating potential interfacial behavior. Lastly, a discussion of

carbon fiber mechanical performance with respect to structural hierarchy qualitative and quantitative interpretation is included.

1.1 Introduction

Carbon fiber reinforced polymers (CFRP) have great importance for future and current transportation industries due to their high strength-to-weight ratio and good chemical resistance, both of which are attractive features for improving energy efficiency and durability. However, defining the mechanical properties of heterogeneous, non-linear, and statistically dependent structures such that even simple material selections and performance predictions can be done reliably has proven more elusive than conspicuous. Issues arise from mechanical complexities derived from increasing orders of structural hierarchy coupled with manufacturing processes, i.e. fiber → bundle → impregnated UD tow → multi-directional composite. When defining material performance, specifically in the constitutive relationship, standards and industrial conventions circumvent the initial, pure compositional states by preparing impregnated tows. Thus, commonly documented carbon fiber material properties are of composite tests, rather than the constitutive materials. This technique is well established in ASTM and ISO standards to evaluate mechanical properties, specifically modulus and strength, of continuous carbon fiber strands and has many sound advantages: (1) it is technically simple to prepare and execute, (2) the results are reproducible with small %CV, allowing for qualitative performance comparison to establish reliable quality controls, and (3) fibers will ultimately be formed into composites parts in which the impregnated tow constitutes a meso-structural entity. However, significant drawbacks exist as well in that the actual fiber properties are embedded in the composite itself as a combination of interfacial behavior and statistical distributions (i.e. fiber bundle) of uniformity, modulus, and

strength. As a result, one must determine ambiguously if the impregnated tow test accurately describes the performance of an embedded structural unit inside a composite part subjected to a wide range of potential manufacturing conditions. It is well-established that discrepancies between fiber and tow mechanical performances using standardized approaches exist. A ~20% increase in measured failure stress is common from the average (N≈38) single fiber test to the impregnated tow test. Hence, the tow test is not conservative relative to single fiber performance, which suggests that performance modeling of composite parts using mechanical properties derived from the conventional standards would result in a non-conservative prediction of actual performance. Moreover, this draws into question the validity of fiber performance metrics, specifically for the novel, newly developed Low-Cost Carbon Fibers (LCCF) [1], when using standardized approaches to validate and compare mechanical specifications.

In this study, a multiscale investigation of a commercial 24k carbon fiber tow utilizing hierarchical levels of mechanical characterization including single fiber tensile testing, single fiber fragmentation, and impregnated fiber strands is used to evaluate the structure-property relationship for carbon fiber tows [2-4]. The mechanical properties from impregnated strands described herein were obtained by two conventional, albeit different, techniques commonly used by major industrial carbon fiber suppliers both which satisfy ASTM and ISO standard requirements. A novel empirical variable extracted from the impregnated tow stress/strain relationship is developed here, which draws on the fundamental non-linear elastic constitutive behavior of carbon fibers to decouple the fiber/matrix interfacial mechanical interaction during tensile testing.

1.2 Materials and Methods

1.2.1 Materials

A commercially available, standard modulus 24k carbon fiber, Epon 862 epoxy matrix with the viscosity reducing additive Cardura E10 (6.49:1), and Epikure W (3.9:1) bisphenol-F hardener were selected for this study. Impregnation of tows was performed using 2 different methods compliant with ASTM D4018-11 standard, specifically a manual (Method 1) and an automated (Method 2) method [5-9]. Method 1, detailed in Figure 1, wets fibers by manual immersion of the fiber tow in a resin reservoir. Sufficient time and careful perturbation was provided to assure complete fiber wetting. To initiate collimation and allow the 42 in. tow to be easily drawn through a 1.55 mm diameter nozzle (Wilton #2) for excess resin removal, the tip of the tow was submerged briefly in acetone. After resin removal, the tow was mounted to a custom aluminum rack, which clamped the ends of the tow maintaining tension during the oven curing process.

Method 2, demonstrated in Figure 1, used automated impregnation by a custom machine with variable winding speed ability to pull tows through a resin bath, squeeze off excess resin through multiple roller paths, and wind the composites tows under tension on a rack for oven curing. The rollers play a critical role to tension the tow and allow collimation while thoroughly wetting and maintaining resin content. For both methods the strands were cured in the oven at 93 °C for 1 hour and then ramped up to 180 °C for 1.5 hours, after which 9 in. specimens for tensile testing were extracted. Unsized samples were made by desizing 42in lengths of tow with acetone. The samples were infused and cured using the manual method. Lastly, dry fiber tows without resin were prepared on the automated instrument such that the tow was tensioned and

collected onto the spindle without passing through the resin bath [10]. The cross section of the fiber tows was determined by dividing Mass per Unit Length (MUL) by the fiber density obtained from a gas pycnometer (AccuPyc II 1340). The resin content for method 1 was determined using equation 1 where MUL_i is the mass per unit length of consolidated fiber [5].

$$RC = 100 * (1 - \frac{MUL}{MUL_i}) \quad (1)$$

1.2.2 Imaging

Short axial regions of the infused flat and round tows were imaged using optical microscopy (Keyence VHX-2000E). Scanning electron microscopy (SEM, Leo 1525) was used to view the cross-sectional areas and diameters of single filaments.

1.2.3 Mechanical Testing

1. **Single Filament**

   Thirty-eight individual single carbon filaments were evaluated using a MTS Nano Bionix Universal Testing Machine (UTM) based on ASTM C 1557-03 and ISO 11566 standards shown in Figure 3. The Nano UTM allows for precise mechanical property data (1nm displacement and 50nN load resolution) governed by a capacitance gage for displacement and electromagnet to apply load at Nano-resolution [11-15]. The diameter of the single filaments was obtained with the SEM. Following mechanical testing, a two parameter Weibull distribution method was used to evaluate tensile mechanical behavior [16].

2. Single Fiber Fragmentation

Eleven SFFT specimens were prepared, where a pretensioned single fiber using a metallic weight was embedded into the resin using a dogbone shape aluminum template shown in Figure 3. The SFFT, based on techniques used in prior studies [17-19], was performed using a custom mechanical load frame where a micro tensile load was applied to the specimen until saturation and fiber fractures were observed utilizing a polarized light microscope (Olympus BX53M). Fiber fractures and delamination zones are measured at saturation, where the length of fractured fibers is used to determine the interfacial shear strength using the Tyson-Kelly equation:

$$\tau = \frac{\sigma_{f*d}}{2 * l_c} \tag{2}$$

Where τ is the interfacial shear strength (IFSS), σ_f is the failure stress of the fiber, d is the diameter of the fiber, and l_c the critical length of the fiber[18].

3. Mechanical Testing of Tows

The carbon fiber tows strands (Figure 3) derived from manual (10 samples), automated (12 samples), unsized (9 samples), and dry methods (12 samples) were mechanically tested using a 25 kN load cell capacity MTS servo-hydraulic with a crosshead rate of 30 mm/minute. Tow samples were sandwiched with epoxy between glass fiber (G10) composites tabs at the ends creating 150mm gage regions for tensile testing. The glass fiber tabs were gripped in hydraulic jaws at 1 ksi. A 1 inch gage length clip extensometer (MTS 634, 12E-24) was centrally attached along the axis of the sample for strain measurement [20]. Data was acquired at 100 Hz for all tow samples tested here. To compare the performance of the tows, a linear density/density based

cross-sectional area measurement was used. The average fiber diameter was approximated by assuming the tow comprises of 24k round filaments. Acoustic emission (Mistras Micro II digital AE system) was used in conjunction to tensile testing. Sensors were placed on the bottom tab without touching the grips. The acoustic emission was started 5 seconds before the tensile test to gather baseline noise to ensure accurate data analysis of the noise and hits received.

1.3 Results and Discussion

1.3.1 Single Fiber Analysis

Single fibers were tested to give a baseline understanding of the commercial fiber being used. The impact of the single fiber properties on the proposed limit state stress is very important and needed to be determined accurately with the Nano UTM. Assuming the weakest link theory applies, Weibull analysis (Figure 5) was performed giving shape and scale parameters 4.5905(m) and 4849(σ_0) respectively. Single fiber fragmentation testing (SFFT) demonstrating the interaction of the interface showed a IFSS of 27.01 MPa due to the high number of fractures with an average fragmentation length of 438.5 μm shown in Table 1. The delamination zones are quite minimal suggesting suitable adhesion between fiber and resin. This phenomenon can be further observed as shown in Figure 5 where the birefringence from resulting strain shows local stress propagation into the resin [18]. In comparison with other reported data (roughly ~45 MPa), this IFSS and fragmentation length is low [21].

1.3.2 Cross-sectional area comparison using Density/Linear Density and SEM

To determine the failure stress of the infused samples, a cross-sectional area of the fiber is required. The typical method used is taking the fiber density and dividing it by the fiber linear density. Table 2 shows fiber diameter comparisons based on two approaches using density-based measurements and scanning electron microscopy (SEM) shown in Figure 6. The general linear density and density approach estimated an individual fiber diameter of ~7.04 microns. Fiber diameters were measured using an image processing software (ImageJ) for thirty fibers averaging to 7.12 microns showing good agreement with linear density approach based on the ASTM standard method.

1.3.3 Infused tow analysis

The average failure stress, taken as the maximum stress achieved during tensile extension, was 5,202 ±102 MPa for the round tows prepared by manual method and 4,904 ± 237 MPa for flat tows prepared by the automated method. A two-sample t-test with respect to the average failure stresses with the zero-null hypothesis gives t=3.94 and less than 1% probability the hypothesis is true, suggesting the difference of these means is statistically significant and that the round tow will produce statistically higher failure stresses for the same fiber, matrix and curing cycles. Furthermore, the %CV in failure stress for the flat tow was 4.8% against 1.9% for the round tow, which indicates the creation of more surface area leads to an increased probability of random surface crack initiation, indicating that the reduction in failure stress observed was a result of the augmented cross-section. The average moduli of the round and flat are 229 ± 3 and 231 ± 4 GPa, respectively. However, a t test for the these means t=1.34 indicates there is insufficient evidence to reject the null hypothesis that the means are equal. Figure 7 demonstrates

the distribution of the failure stress and modulus data for the round and flat tows, and visually reinforces conclusions obtained from the statistical analysis.

Composite stress/strain and modulus/strain curves of round, flat, and dry tows were created by interpolating the data to a common strain increment and averaging the corresponding stresses and are presented in Figure 8. This procedure provided the most simplified and suitable basis for contrasting the performance of the tows without the individual, stochastic differences between single test specimens. It is important to note that due to the heterogeneous micro-structure and internal stress distributions in impregnated tows, there results sudden strain jumps associated with development and propagation of cracks occurring along the gage length, thereby inducing discontinuities in the stress/strain relationships. Local discrete differentiation over a strain window of 0.0004 causes strain discontinuities to be apparent through large sudden drops in the modulus as shown in Figure 8.

In order to account for stochastic strain discontinuities in the mechanical behavior and produce an accurate summary of the mechanical response, composite curves of all the samples tested here were made by averaging interpolated stress values. The composites stress/strain curves with respect to the unmodified data is given in Figure 9. Initially, at low stresses, all the tows behave similarly, but as the stress magnitude increases and random failures occur with the individual strands, the responses begin to separate, which appears as a fanning out of the data at high stress levels in Figure 9.

Using the composite stress/strain curves, modulus curves were produced by linear fit over a strain window of 0.0004 and are given in Figure 10 A & B for multiple tow types. The stress/strain behavior of all tows (dry and impregnated) and single fiber are initially identical, but

with increasing stress magnitude the dry tow begins to decrease in modulus and fall below the single fiber and impregnated tows. However, comparing the single fiber tensile stress/strain relationship with that of the resin impregnated or dry fiber tows, a deviation is noticed at high strain magnitudes such that single fiber modulus continues to increase, while tow moduli decrease.

The tensile mechanical behavior of a single carbon fiber of any precursor is most accurately described as non-linear elastic up to failure, the peak load achieved during tensile extension [12, 13]. As such, the modulus is typically described by a linear relationship with strain as in Eq. 3, where γE_0 and E_0 are the slope and y-intercept, respectively.

$$E(\varepsilon) = \gamma E_0 + E_0 \tag{3}$$

This relationship indicates that the modulus continuously increases at the same rate with strain until failure. This stiffening behavior of single fibers in Figure 10B has been measured in this work without the reliance of discrete data differentiation but rather using the dynamic testing approach previously introduced [13]. Furthermore, if the modulus is linear, the axial stress/strain response is best modeled as parabolic. Composite modulus/strain curves demonstrating the average of 35 single fiber tensile tests in Figure 10B, clearly represent the increasing modulus with strain up to sample failure. Hence, for a single carbon fiber in axial extension the modulus is continuously increasing.

The deviation of tensile mechanical response of the composite fiber tows and single fiber can be used to define a new stress parameter, stated for the first time here as the limit stress, which indicates the accumulation of inter-fiber effects and damage overtaking the stiffening effect related the constitutive behavior of single carbon fibers. Similar to the yield stress in

ductile materials indicating the ceasing of elastic material response, the limit stress indicates the ceasing of the non-linear elastic response. A graphical technique was developed here to determine the limit stress and was applied to three composite tows (flat tow, round tow, unsized-round tow) of different manufacturing origin to produce predictable and observable changes. The following steps outline the procedure used for calculating the limit stress on a composite tow:

1. The initial slope of the modulus is determined by best fit of the modulus data.
2. The linear fit modulus is integrated to produce an approximated non-linear elastic stress/strain relationship.
3. The approximated stress/strain relationship is offset from the measured stress/strain response. (A 0.0002 strain offset was used in this study.)
4. The crossing point of the approximated stress/strain data and the actual measured stress/strain data is calculated, giving the limit stress.

This could also give insight on the interfacial properties of the fiber and resin. The authors hypothesis is that when you have good interfacial behavior this leads to better stress distribution and vice versa. A lower limit stress demonstrates that the sample deviated from nonlinearity sooner than that of a higher limit stress. For example, the round tow and the unsized round tow were manufactured in a very similar fashion so that the only difference is the presence/absence of sizing. This represents strong interfacial difference between the samples. The nonlinearity shown in Figure 11 B and C demonstrates that the unsized tow composite demonstrates mechanical properties closer to the true properties of the single fiber. This could be due to the potential delamination that occurs when cracks propagate leading to less load sharing through the matrix. This allows the fibers in the unsized sample to behave more like remotely-loaded single

fiber. The distribution of stress is affected by this change in the interface which manifests itself as a decrease in limit stress from the round tow to the unsized round tow. This behavior is not noticeable in the ultimate failure stress. Further study will be required to better understand this phenomenon.

Acoustic emission (AE) is a non-destructive evaluation technique used to analyze fractures or defects. A few tensile tests were performed with AE to gain more confidence of the limit stress parameter proposed by showing fiber fracture before failure. Figure 12 shows a single example test for the various tow tests completed with acoustic emission. The round and flat tows show an increase in the acoustic energy starting at ~1.5% failure strain indicating that fracturing is occurring within the sample but is not yet shown as a drop in load. The unsized round tow has extra peaks in the acoustic energy before failure which potentially demonstrates bundles of fiber breakage at once or extensive crack propagation through the sample. This information suggests that AE may be able to identify interface-based failures are not otherwise easily captured through the gathered stress-strain data. Further studies using AE could be used to isolate the fiber breakage signature peaks from matrix cracking to develop a better understanding of when fibers are fracturing.

It is also important to investigate variations in the other mechanical properties of the various methods studied. An understanding of the effects of the manual and automated methods is of interest due to both being allowed within the standard. The flat infused tow has a lower ultimate failure stress (~280 MPa) than the round infused tow shown in Table 3. The flat tows had a higher standard deviation than the round tows which indicates the consolidation of the manual round tows is more consistent than that of the automated flat tows. This could be attributed to

difference in cross-section geometry between round and flat samples shown in Figure 13. The stress transfer capability within the flat infused tows could be hindered due to the non-constant distance from edge-to-edge. The round infused tows have a more uniform edge-to-edge distance to reduce stress concentrations at the edge, which could help improve the stress transfer from fiber to fiber thus improving the round tow tensile strength.

Another significant potential for variation between the methods is the tensioning of the tow during the manual and automated processes. Figure 14 shows an example of potential non-tensioned fibers in the carbon fiber tow after being impregnated, tensioned, and cured. This could affect the overall mechanical properties of the infused tow due to unused energy (example of the inter-fiber interaction discussed in the limit stress section). Once the infused tow is cured with some non-tensioned individual fibers, the load at first fracture is expected to decrease as the non-tensioned fibers will not fully bear the load. Consecutive fractures will occur at lower loads as the load is shared with the surrounding un-failed fibers. It is feasible to expect that greater plasticity will occur, as the non-tensioned fibers become elongated during loading. These un-failed fibers will continue to bear load, but the global stress will remain low until final fracture. This would be especially true for the dry tow and explains the decreased failure stress. This also could have a compounding effect on the tensile strength when considered alongside the cross-sectional area variation previously discussed.

1.4 Conclusions

A multiscale analysis using commercial carbon fiber was performed including single fiber, single fiber fragmentation, and impregnated fiber tow testing. The carbon fiber single filaments were assumed to be round, which was confirmed using SEM and optical microscopy.

The ASTM D4018-11 standard was used to prepare the impregnated fiber tow samples using the suggested automated and manual methods. There was about a 6% increase from the automated method to the manual method, which could suggest better stress transfer and lessened edge effects for the round samples opposed to the flat samples. A new method for reporting stress values, named the limit state stress, was proposed to be considered alongside the ultimate failure stress typically reported. The limit state stress may be indicative of interfacial behavior, but further study is required. Single filament data showed that the failure and storage modulus of single fibers plays a major role in the new limit state stress proposed. Acoustic emission was used to illustrate that fiber failures and matrix fracturing occurs between the limit stress and ultimate failure stress, a phenomenon that cannot be visually confirmed. The infused tows exhibited a rise in acoustic energy at the strain at which the limit stress was proposed for the flat, round, and unsized round sample geometries.

1.5 Appendix

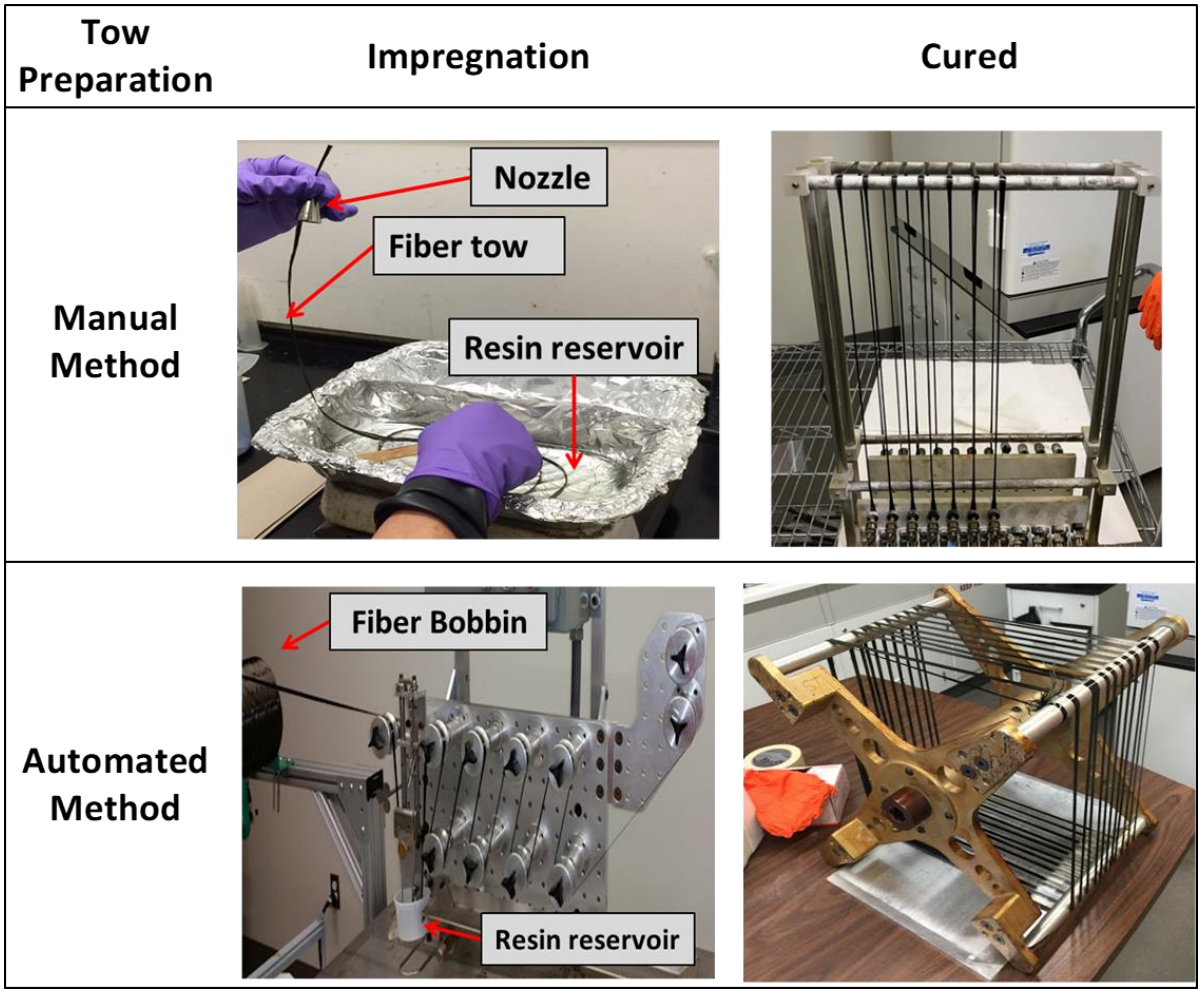


Figure 1 - Example setup of impregnation process using the manual and automated methods described within the ASTM D4018.

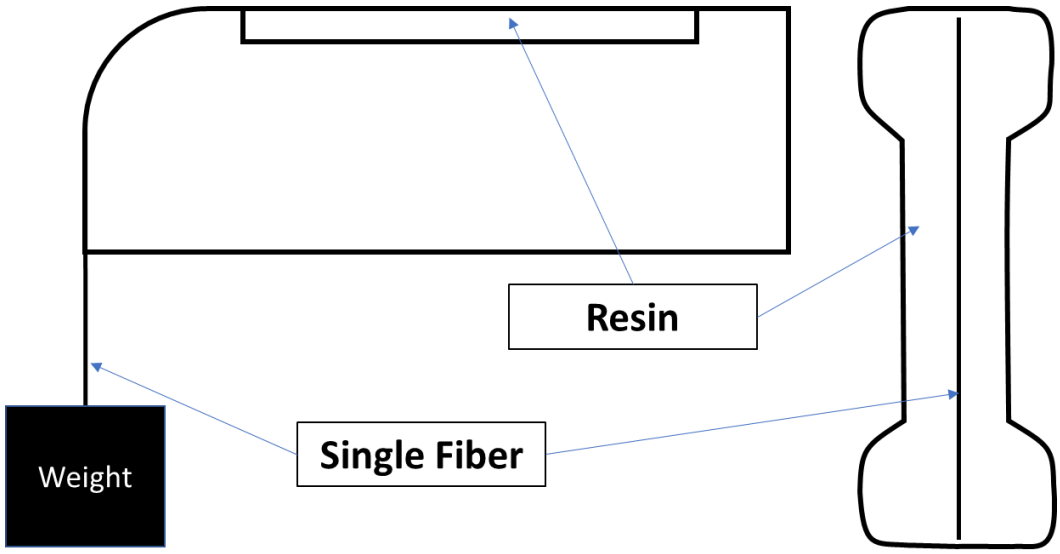


Figure 2 - Single fiber fragmentation mold demonstrating pre-tensioning and impregnation of the single carbon fiber.

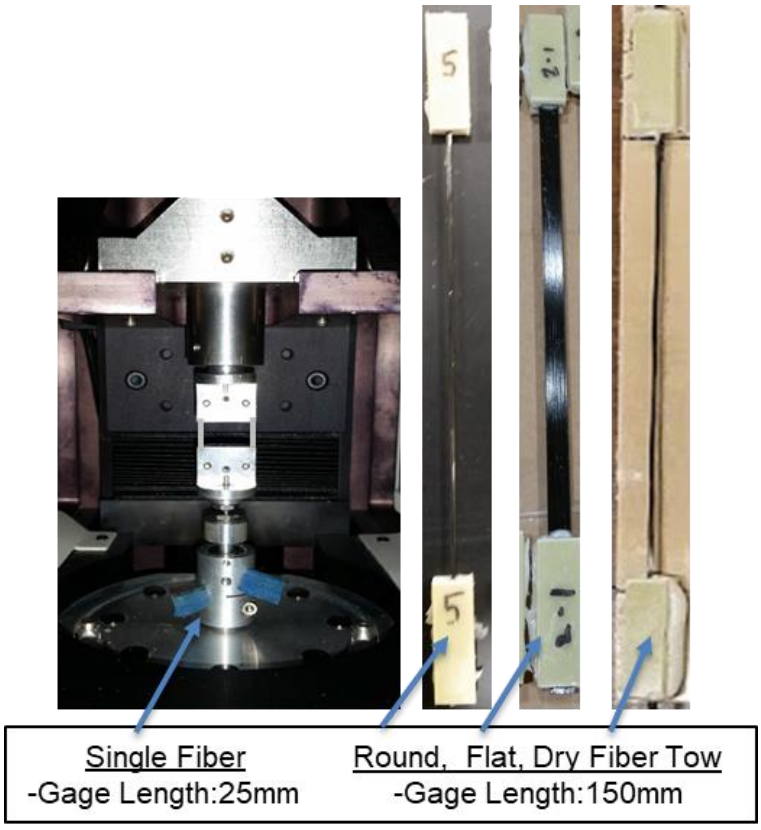


Figure 3 - Example tabbed single filament carbon fiber and impregnated carbon fiber tows

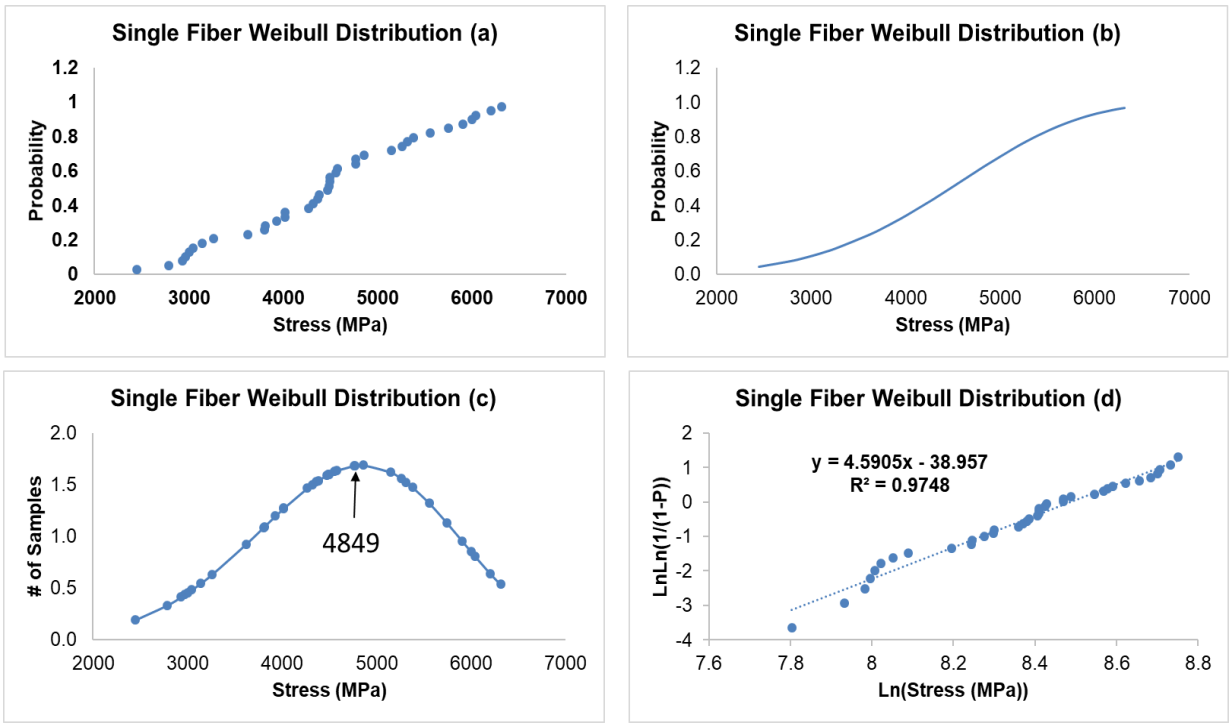


Figure 4 - Single filament Weibull statistical distribution demonstrating

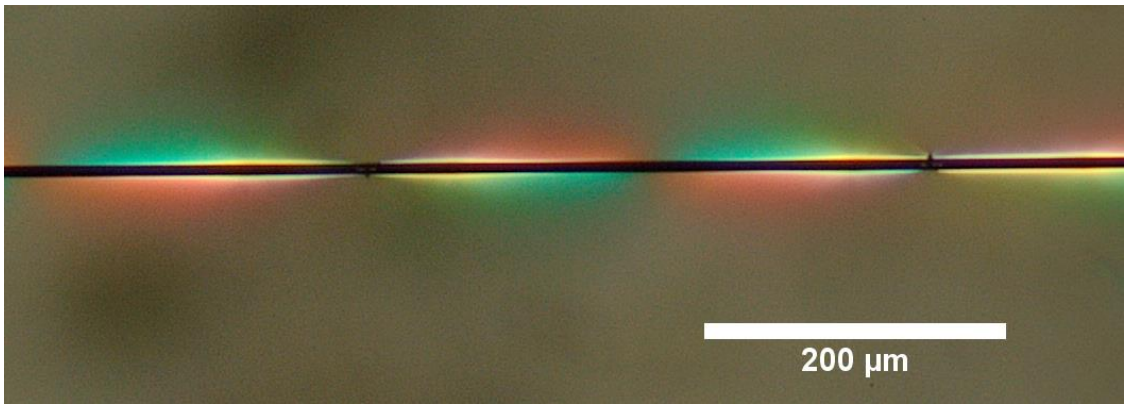


Figure 5 - Optical micrograph showing fiber fractures exhibiting crack propagation and interfacial mechanical failure along the fiber.

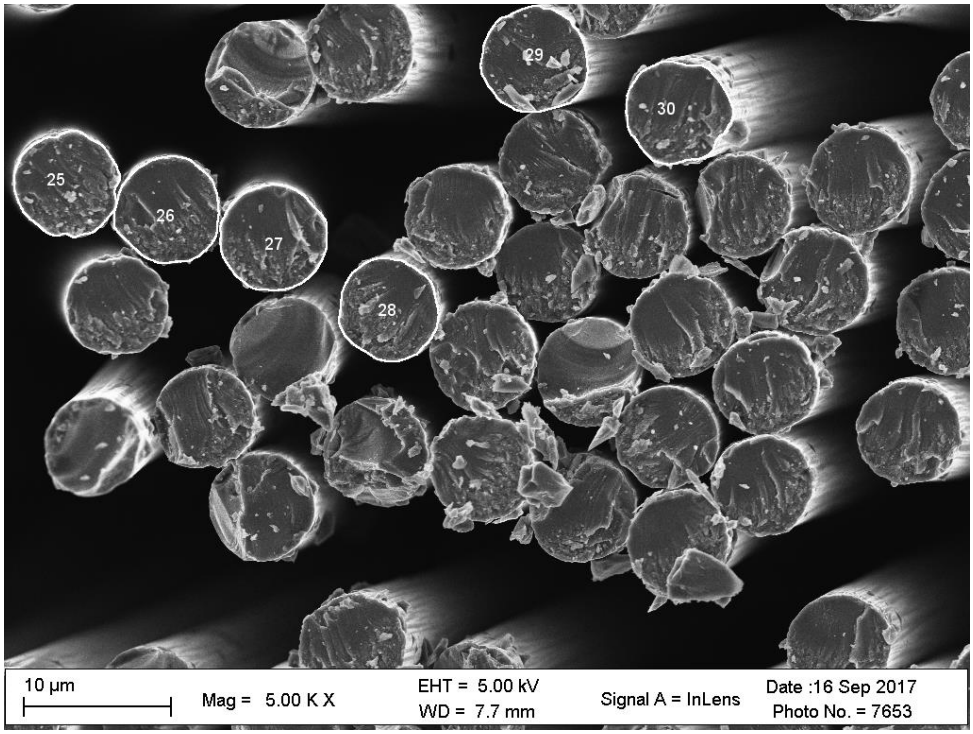


Figure 6 - SEM micrograph showing cross-section of commercial grade 24k carbon fiber

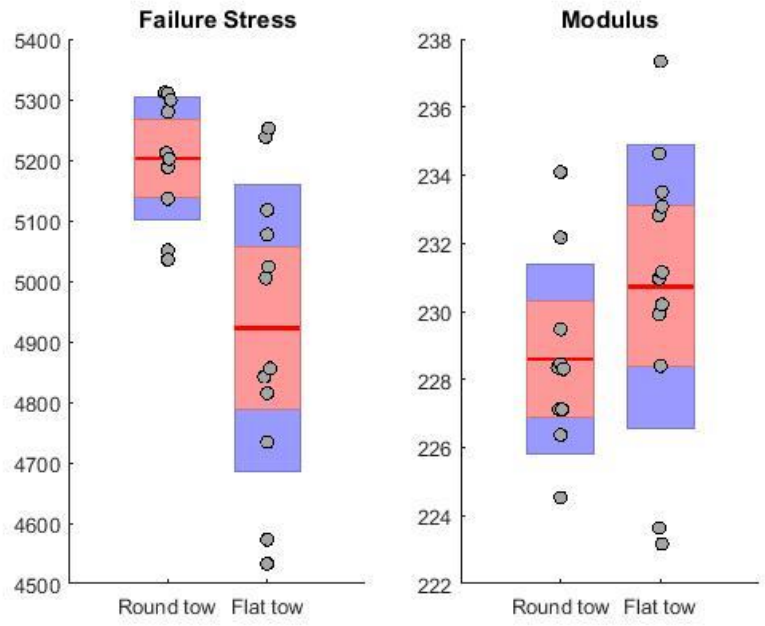


Figure 7 - Distribution of Failure Stress and Modulus for flat and round tows, demonstrating increased failure stress of the round (manual) tow preparation against the flat (automated) tow preparation, and the statistically indistinguishable difference in modulus.

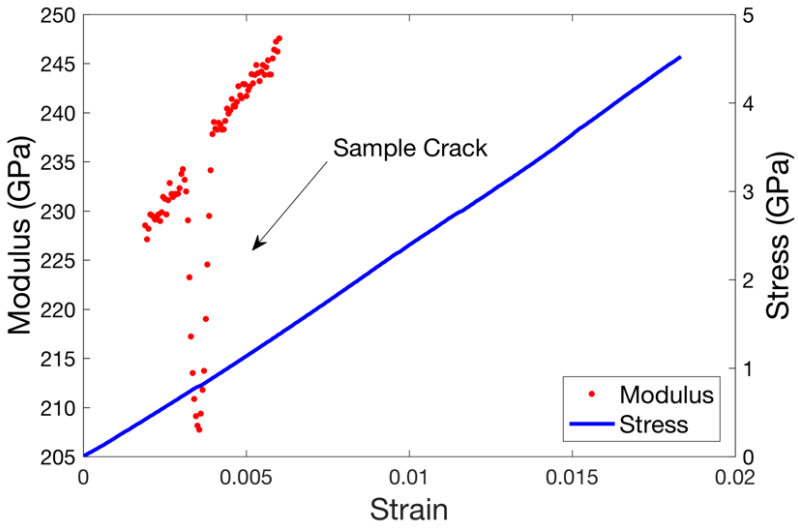


Figure 8 - Example mechanical response for single flat tow test, demonstrating a modulus drop associated with cracking and delamination of fiber and resin during tensile deformation.

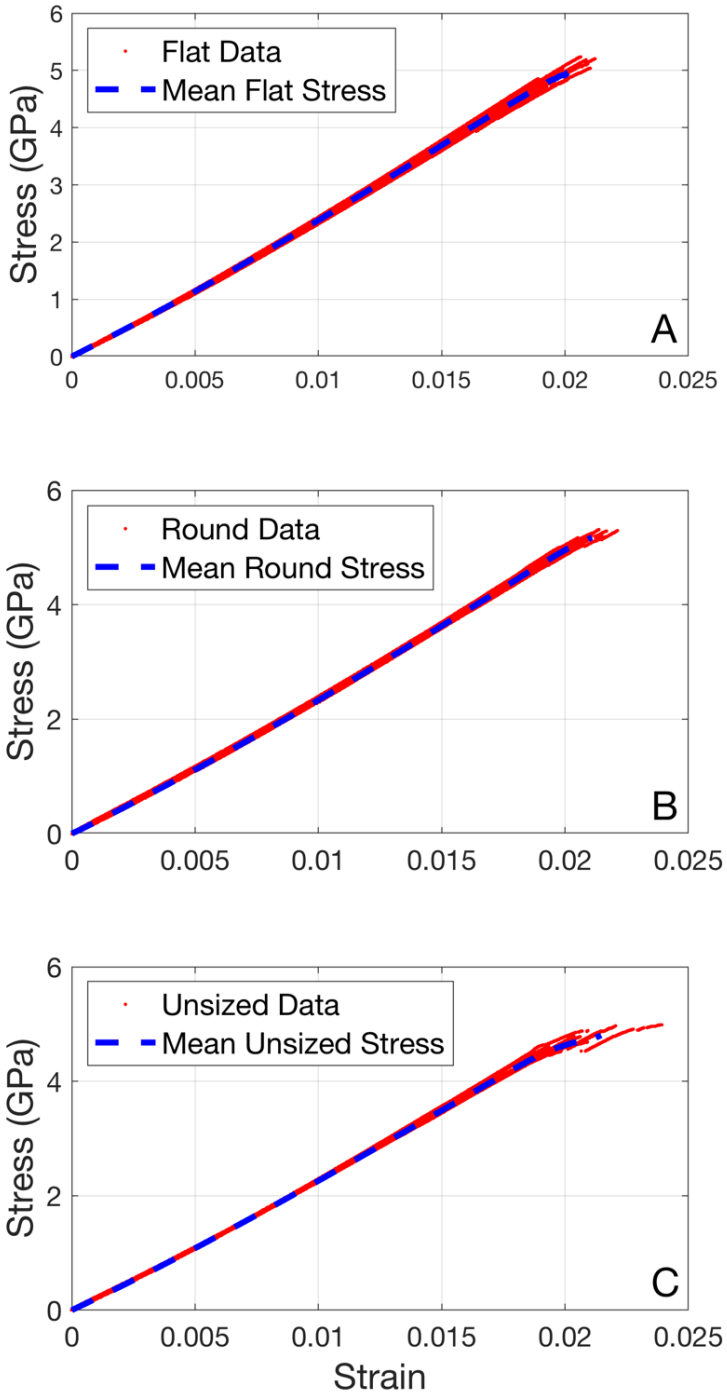


Figure 9 - The composite stress/strain response for (A) flat, (B) round, and (C) unisized round impregnated fiber tows relative to all the raw data.

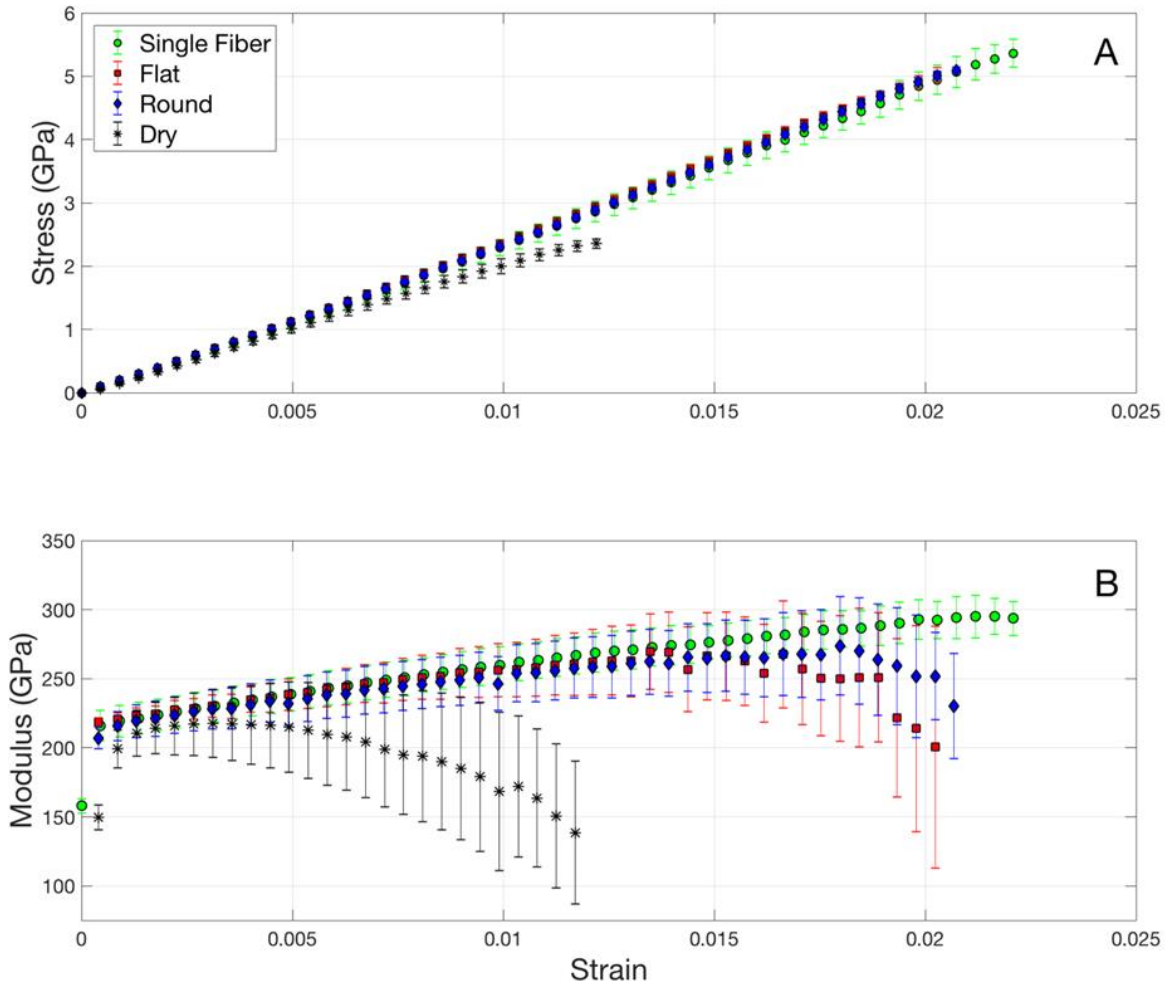


Figure 10 - Composite stress/strain and modulus/strain response for samples examined here, noting that the single fiber modulus continues to increase with strain magnitude, while tow moduli begin to decrease as sample damage accumulates.

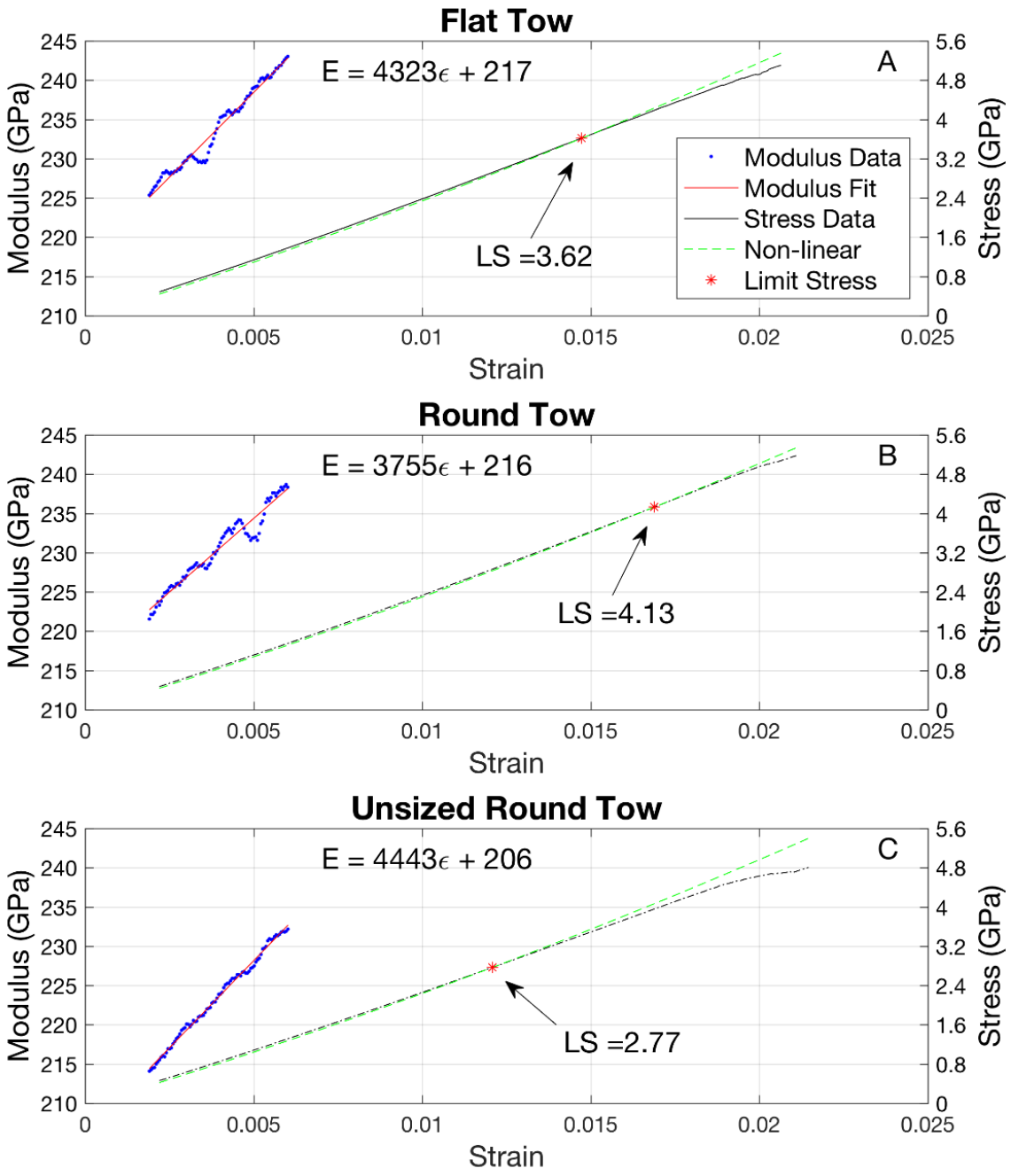


Figure 11 – Graphical demonstration of limit stress for (A) flat, (B) round, and (C) unisized round impregnated fiber tows. The decrease in the limit stress for the unsized round and flat tow relative to the round tow indicates the increase inter-fiber effects from the manufacturing technique used.

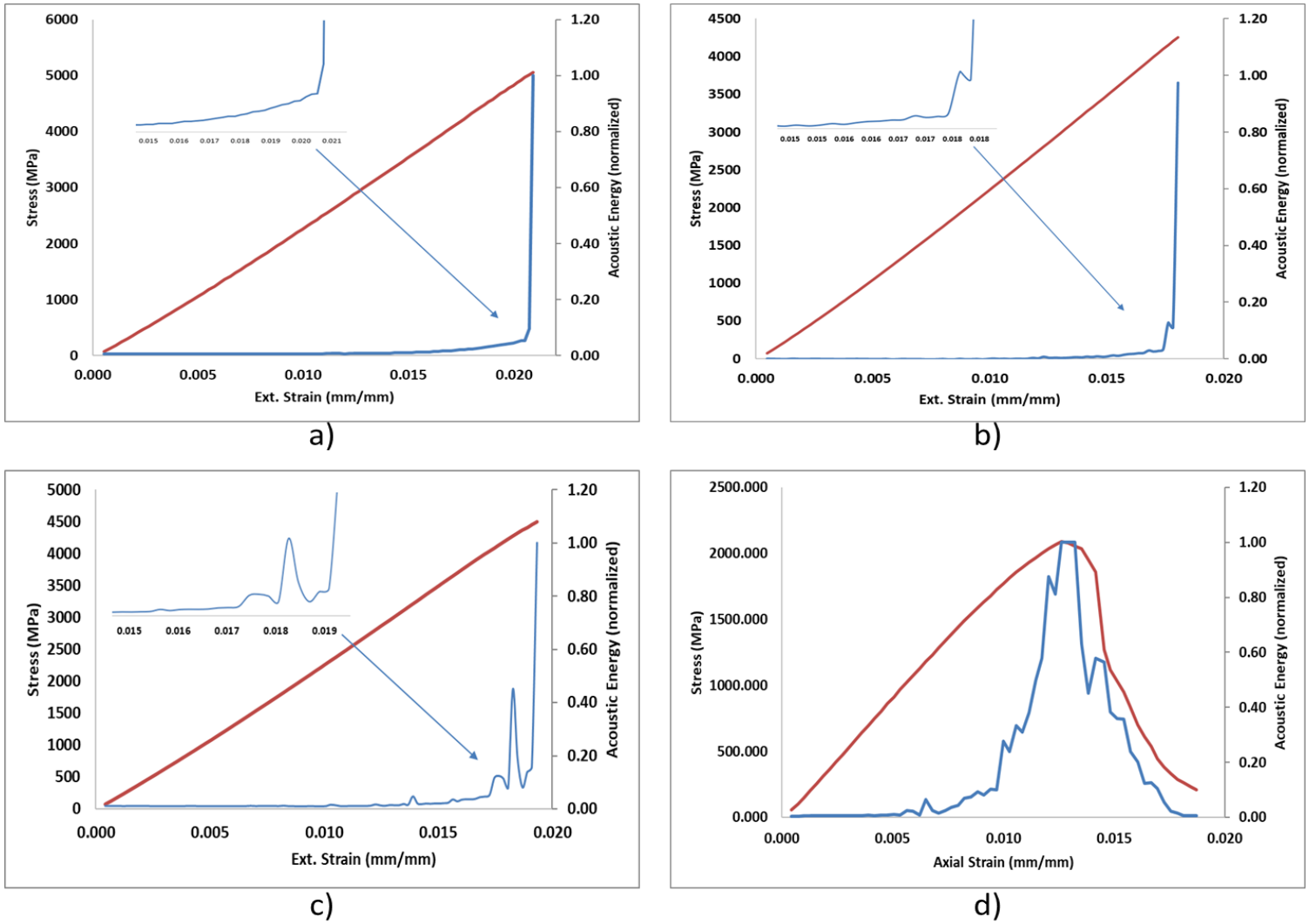


Figure 12 - Stress strain data with normalized acoustic energy layover demonstrating fiber and matrix fracturing for a) sized round infused tow b) sized flat infused tow c) unsized round infused tow and d) dry uninfused tow

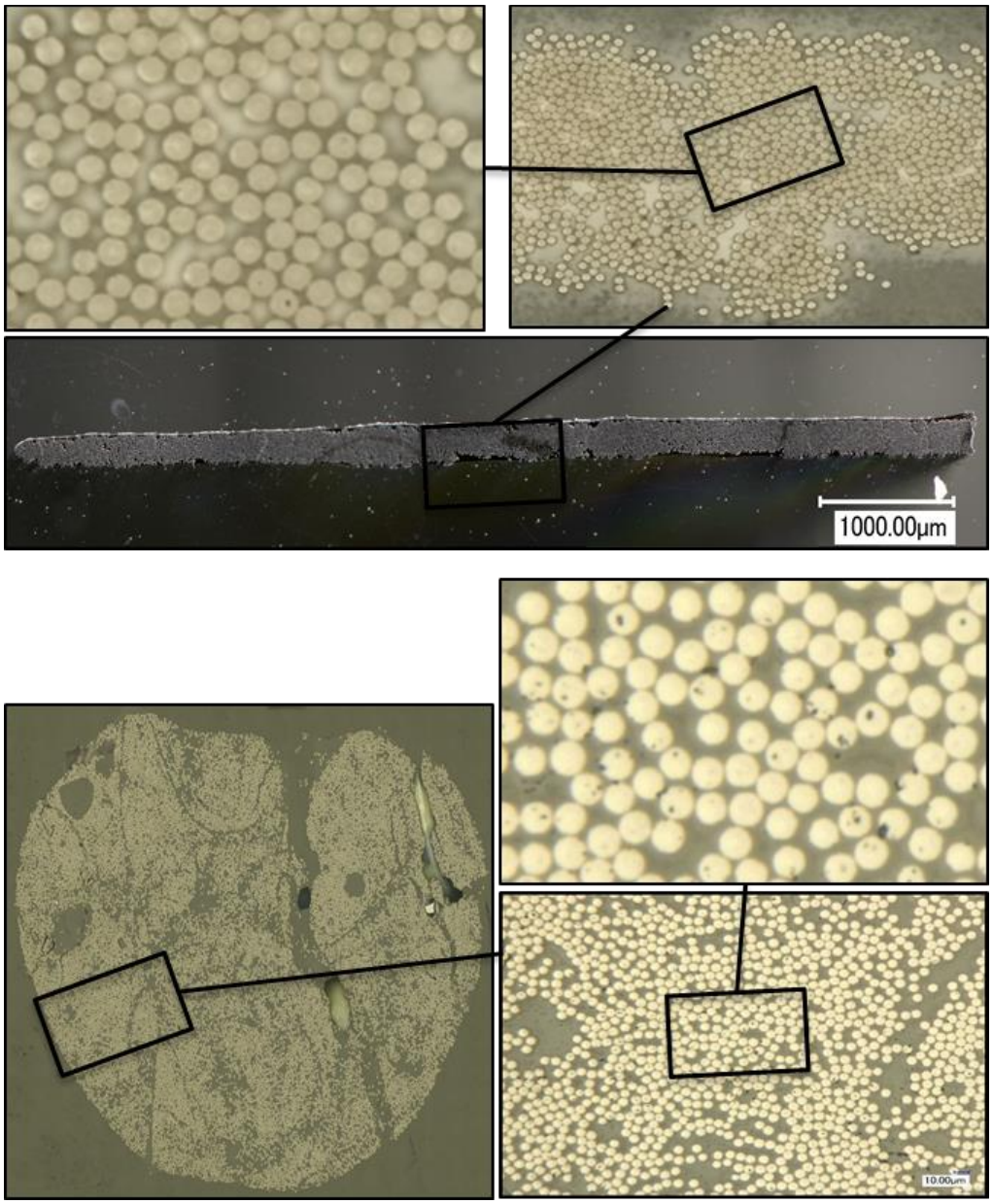


Figure 13 - Microscopy showing example cross sections of the infused flat and round tow demonstrating resin voids, fiber packing, and overall structure.

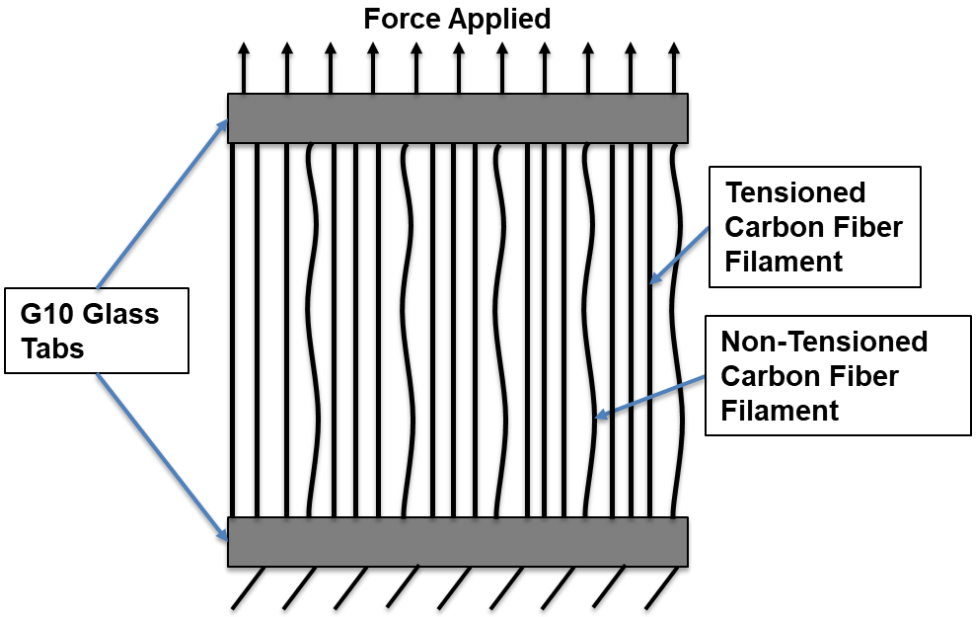


Figure 14 - Potential variation in tensioning of the fibers that could occur during impregnation process.

Table 1 Single fiber fragmentation data

Average Fragmentation Length	Standard Deviation	Critical Length	Interfacial Shear Strength	Failure Stress	l/d
μm	μm	μm	MPa	MPa	
438.47	166.36	584.63	27.01	4433.71	75.83

Table 2 Cross-sectional area calculations based on linear density/density and SEM average diameter

Linear Density	Density	Tow Area	Fiber Area	Fiber Diameter
g/cm	g/cm^2	mm^2	mm^2	microns
0.0166	1.7800	0.9334	3.89*10^-05	7.04
*Calculated based on measured SEM diameter 30 sample average		*Tow Area	*Fiber Area	SEM Diameter
		mm^2	mm^2	microns
		0.9563	3.99*10^-05	7.12

Table 3 Comparison of mechanical properties of single filament, manual, automated, and dry methods

Sample	Average Ultimate Failure Stress (MPa)	Std. Dev. (MPa)	Average Limit Stress (MPa)	Average Modulus (GPa)	Std. Dev. (GPa)	Average Failure Strain (mm/mm)	Std. Dev. (mm/mm)
Single Filament	4434	1045	-	260	21	1.85%	0.39%
Unsized (Manual)	4739	287	2770	218	10	2.14%	0.20%
Method 1 (Manual)	5213	137	4130	229	3	2.29%	0.09%
Method 2 (Automated)	4909	229	3620	231	4	2.26%	0.15%
Method 3 (Dry)	2163	603	-	217	11	1.23%	0.16%

CHAPTER 2
THERMAL-MECHANICAL ANALYSIS OF TEXTILE PAN AND THE STRUCTURE-PROPERTY-PROCESS RELATIONSHIP

This chapter is a slightly different version of a paper with the same title that will be submitted for journal publication by 2019 by Joshua D. Crabtree, Dayakar Penumadu, David Harper, James Eun, and Merlin Theodore.

My primary contributions to this paper include: (i) development of the problem into a work, (ii) identification of the study areas, (iii) gathering and reviewing of literature, (iv) sampling, processing, and analyzing data, (v) pulling various contributions into a single paper, (vi) writing.

Abstract

Carbon fiber reinforced composites are highly attractive to the automotive, sporting goods, and aerospace industries due to their high strength, low weight, thermal, physical properties. However, carbon fiber is relatively cost-prohibitive due to its manufacturability, namely the precursor. Low-cost carbon fibers have been developed recently however critical properties including structure-property relationships are not well understood. In this study, three PAN-based precursor and carbon fiber types with different spin finishes were characterized for process-property relationships. Precursor and oxidized PAN fiber microstructure were analyzed using FT-IR for bond characterization, X-ray diffraction for crystallinity, SEM microscopy for microstructure features of importance and Thermal properties including TGA and DSC. Mechanical properties such as modulus, strength, failure strain is included for single fiber and tow. The results indicate the role of spin finish and tenacity is not significant considering the variation of the properties expected from low-cost carbon fiber. The results indicate the role of

spin finish and tenacity is not significant considering the variation of the properties expected from low cost carbon fiber.

2.1 Introduction

Carbon fiber reinforced composites are in high demand for automotive and aerospace industries due to desirable properties of high strength/modulus, resistance to corrosion, excellent electrical properties, and low weight. Polyacrylonitrile (PAN) is one of many sources from which carbon fiber can be produced. Due to slightly higher properties, PAN is typically chosen over pitch-based or rayon-based fibers for carbon fiber production [22, 23]. As the demand for carbon fiber continues to increase within industry, there are needs for finding alternative methods to lower the cost while being able to keep up with the production manufacturing standards[24, 25]. One approach that the Carbon Fiber Technology Facility at Oak Ridge National Lab used was selecting a cheaper precursor, specifically a textile grade acrylic fiber which had the potential to cut overall costs by up to 50% [1, 23, 24, 26, 27]. Once a precursor fiber is chosen, it is desirable to understand the structure of the fiber on an atomic scale, as well as the conversion process and the effect on the properties [28-35]. It is understood that a cheaper precursor from the textile industry would have a higher comonomer percentage due to better stretch ratios which lowers the amount of acrylonitrile than that of the commercial precursor, so it is important to have the capability to enhance/optimize the properties and tailor to specific applications [25, 26, 36-39]. A common method used by polyacrylonitrile manufacturers during production is to apply a surface lubricant during the spinning operation called a spin finish. Synthetic fibers lack a natural lubricating oil which is found in natural fibers (wool, cotton, etc.) and thus require this spin finish. The application of spin finish to synthetic fibers is important to reduce the static

charge that can develop due to the fiber to fiber interaction as well as the contact with the metal roller surfaces [40-42]. This can lead to major problems for the manufacturer's process without the dampening of this potential electrostatic charge. The benefits of the spin finish translate to the carbon fiber manufacturer's process as well helping to reduce entanglement of fibers and potential electrical charges that can build up during the conversion process. Another property that textile manufacturers determine is the tenacity of their fiber. This is a type of specific tensile strength of the PAN fiber expressed as breaking load per denier with units of grams/denier. This metric also has a relationship to the modulus of the fiber [43].

In this paper the authors investigate three textile polyacrylonitrile precursor materials, with either tenacity or spin finish variations, to evaluate the thermal-mechanical properties to better understand the oxidation effect and conversion to carbon fiber. Analysis of the spin finish to understand the effect on the mechanical properties was determined. The tenacity was also analyzed to determine an effect if any on the overall mechanical properties.

2.2 Materials and Methods

2.2.1 Materials

The fibers used in this study included three different precursor materials with some modifications received from the Carbon Fiber Technology Facility (CFTF). Each fiber tow consisted of 457,000 individual filaments with a kidney-bean shaped cross-section shown in Figure 15 [44]. Fiber A and Fiber B have the same spin finish with different tenacities. Fiber A and Fiber C have the same tenacity but different spin finish. The fibers were oxidized, stabilized,

and carbonized using the semi-production line at the CFTF, with samples at each stage of the process.

2.2.2 Characterizations

DSC

Differential scanning calorimetry (DSC) was performed to analyze the three precursors and the respective oxidized PAN fibers (OPF). A Perkins Elmer under nitrogen atmosphere and a Mettler Toledo TA1 under air atmosphere were used. A temperature range of 25-500 °C with a heating rate of 100 °C/min and 20 °C/min was consistent on both systems [34]. Two samples for each precursor and OPF were prepared by chopping the fiber and placing about 2.5 mg in the sample cup. The lid was attached with a hole poked in the center to allow for release of volatiles during testing.

TGA

Thermogravimetric analysis (TGA) was performed using a Perkin Elmer Pyris 1. A temperature range of 25-900 °C with a heating rate of 10 °C/min under nitrogen was used.

FT-IR

Fourier Transform Infrared spectroscopy (FTIR) absorption spectra were performed with a Perkins Elmer Spectrum Two FT-IR using a diamond/ZnSe crystal. Using the UATR (universal Attenuated total reflectance) accessory, repeatable force applied to the sample allowed for consistent contact with the crystal. The wavelength range analyzed was 500-4000 nm.

XRD

X-ray diffraction using transmission was collected using a PANalytical X'Pert^3 MRD on the three precursors and their corresponding oxidized pan fibers. Interplanar spacing and

diffraction angles were determined using Equation (1) Bragg's law. Rearranging Equation 1 we can determine the interplanar spacing d in Equation 2. The crystallite size is determined from Equation 3, the Scherrer formula.

$$\lambda = 2dsin(\theta) \quad (1)$$

$$d = \frac{\lambda}{2sin(\theta)} \quad (2)$$

$$L_c = \frac{K\lambda}{Bcos(\theta)} \quad (3)$$

Where λ is the CuKα wavelength (1.541 Å), d is the interplanar spacing, and θ is the diffraction angle, K=0.89 a constant, and B is the FWHM [45].

SEM

Scanning Electron Microscopy (Zeiss Dual Beam FIB/SEM) was used to obtain cross-sectional areas of the carbon fibers for single filament testing.

Density

Density measurements were completed using a Micromeritics Accupyc 1340 II with helium gas. The precursor material and oxidized PAN fiber were dried before measuring the density to remove any moisture present.

Single Filament Testing

Thirty single carbon fiber filaments of fiber A, B, and C were tested using a MTS Nano Bionix Universal Testing Machine (UTM) based on ASTM C 1557-03 and ISO 11566 standards displayed in Figure 16. The Nano UTM is very precise with a 1 nanometer displacement resolution and a 50 nano-newton load resolution. Modified grips help with the accuracy of

mounting and testing of single fibers based on ASTM and ISO standards [11-15]. The Weibull Distribution method was used to analyze the mechanical properties of the three single fiber data sets with a strength and scale parameter [15, 16].

Tow Testing

ASTM D4018-11 was used to prepare infused carbon fiber tows using EPON Resin 862 (Diglycidyl Ether of Bisphenol F) mixed with the viscosity reducer Cardura E10 (Glycidyl Ester) using 6.49:1 ratio. This mixture is then combined with the hardener Epikure Curing Agent W with a 3.9:1 ratio. Samples were infused in a resin bath manually, sufficiently wetting the tow, and pulled through a 2.03 cm diameter nozzle (Wilton #3) to control resin content. The tow is then attached to a custom strand rack and pulled taut to maintain tension through the curing process. Once all samples are attached the rack is placed in the oven and a curing process of 93 °C for 1 hour and then ramped to 180 °C for 1.5 hours. Samples were then cut to 9 in lengths and G10 glass tabs were applied at the ends to give a 150mm gage length shown in Figure 17. Tensile testing was performed on a 25 kN load cell capacity MTS servo-hydraulic with a crosshead rate of 30 mm/minute shown in Figure 16. A 25.4 mm gage length extensometer was used to accurately record strain data.

2.3 Results and Discussion

2.3.1 FT-IR Spectra Analysis

The FT-IR spectra of the three PAN and OPF fibers shown in Figures 18 and 19 show that each of the fibers, regardless of the spin finish and tenacity, are remarkably similar with a few slight differences. This demonstrates good agreement to literature IR spectra for

polyacrylonitrile precursor and oxidized PAN fiber [37, 38, 46, 47]. Many IR peaks for polyacrylonitrile are due to the CH2, C=O, C─O, C─H, and C≡N bonds present. The absorption peaks in the range 2930-2850 cm-1 are from the various C─H bonds [46]. The peak at 2242 cm-1 is related to the nitrile (C≡N) presence [47]. The peaks at 1732 cm-1 and 1166 cm-1 are representative of the comonomers present which is likely vinyl acetate (VA) or methyl acrylate (MA) [39, 47, 48]. Aliphatic CH vibration along the polyacrylonitrile backbone is very clear with the 1452 cm-1 and 1361 cm-1 peaks [37]. According to Sungho Lee et all. the 1070 cm-1 peak could be represented by S=O group potentially remaining from a DMSO solvent [38]. When the precursor is oxidized there are evident peaks that decrease, and new peaks appear as shown in Figure 19. Oxidized PAN fiber IR spectra shows a decrease in the peaks around 2900 cm-1, release of HCN, and 2240 cm-1 and an increase in the peak 1583 cm-1 which is due to the cyclization process that began [39, 47]. During this process there is also dehydrogenation reflected in the decrease of the peak around 1450 cm-1 and the increase of the 1360 cm-1 peak. The 800 cm-1 peak develops from =C-H groups from what appears to be oxygen aromatization due to stabilization in air [37].

2.3.2 X-Ray Diffraction Microstructure

For a more thorough understanding of textile-based PAN microstructure, it is important to determine the baseline of accepted commercial PAN molecular structure. Figure 20 shows the model widely accepted for polyacrylonitrile fiber demonstrating the helical macromolecule, macromolecule orientation and the individual fibril. Given the information of the macromolecule structure of the PAN fiber we can determine that the peak at ~17° in Figure 21 is from the planar spacing shown in Figure 20a). The peak at ~29° can be determined to fibril diffraction from

Figure 20b) between the paracystalline domain and amorphous domain. In Figure 21 a new peak develops at ~25.5° in the OPF that wasn't in the precursor. This is due to the transformation occurring in the polymer structure which corresponds to the graphitic structure [49].

The X-ray diffraction results and orientation of the three textile PAN precursors and oxidized fibers were all extremely similar and an example of the peaks are shown in Figure 22. Fiber B in Figure 22a has less intensity than fiber A or C at the same peak locations which could indicate less orientation for the higher tenacity fiber. Figure 22b shows fiber A and B are practically identical with a higher intensity in peak 1 than peak 2. This is not the case with fiber C which shows peak 2 overtake peak 1 in intensity. This could be an indicator of oxidation being marginally better because of the more proper formation of this pre-graphitic peak [49]. The orientation of the fibers shown in Figure 22c and 22d indicate that each precursor and OPF fibers are very well orientated. Table 22 demonstrates how similar the 2θ peak locations for the measured XRD patterns are as well as show the slight differences in the chi/azimuth scan of the orientation. Using the 2θ information, the structural parameters of the d-spacing was also determined. Overall the spin finish and tenacity didn't seem to have an impact on the atomic structure of the precursor or the oxidized PAN fiber and the textile-based material is highly similar to its commercial counterpart.

2.3.3 Thermal Characterization

Thermogravimetric analysis (TGA) shows the moisture and various volatiles present within the fiber samples. It also offers an insight to how the fiber will breakdown when exposed to thermal treatment as well as show the mass loss. Figure 23 shows the mass loss trend for all three precursors and oxidized PAN fibers. There is a consistent trend that each of the precursors

at 345 °C begins to lose mass which indicates a chemical reaction beginning which releases volatile gases and shows good agreement with the DSC curves shown in Figure 11. At 500 °C the fiber is now starting to oxidize while releasing HCN and NH_3 which shows stabilization. The oxidized PAN fiber TGA in Figure 23 shows a decrease around 100 °C which can be attributed to moisture. Each fiber type indicated comparable trends as the mass loss occurred through the heating cycle.

A study of how the environment and heating rate affects the thermal analysis of the precursor and OPF fibers shown in Figure 24. A comparison between a fast heating rate of 100 °C/min and a slow heating rate of 20 °C/min demonstrated some variation, especially in the nitrogen atmosphere. The rate didn't seem to have much of an effect on the air atmosphere, but the location of the peaks and enthalpies didn't seem to match literature. It was determined that for this research purpose, the nitrogen 100 °C/min produced the most accurate data. The differential scanning calorimetry (DSC) curves for the precursor A, B, and C showed similar onset temperatures and measured enthalpies shown in Table 5 and Figure 25. Fiber A contains a more intense peak which could attribute to the spin finish, but it is unlikely since Fiber B has the same spin finish with less intensity. The peaks for each of the fiber types are virtually identical showing that spin finish and tenacity ultimately didn't affect the thermal precursor properties.

Analysis of the oxidized PAN fiber is shown in Figure 26 for each of the fiber types. There are two distinctive peaks for each of the fiber types. The first broad peak appears at about 100 °C which are not observed in the precursor DSC data. This could be attributed to the heat input needed for evaporation of moisture. After oxidation there is a change in the structure of the polymer and is more susceptible to pick-up moisture. The second peak is around 350°C with a

little more variation in the OPF data then that of the precursor, but still very comparable. The enthalpy ratios of the OPF/precursor for fiber A, B, and C are 64%, 79%, and 78% respectively. This is a potential metric to indicate a degree of oxidation and to help determine if the fiber oxidation is the best it can be to maximize the mechanical properties once converted to carbon fiber.

Density measurements were taken of the precursor and OPF following the procedure mentioned in characterizations. It is notable that the densities among the fiber types are really similar to each other at the precursor and OPF stage. There is an increase of ~.2 in density from precursor to OPF due to the oxidation of the fiber. The carbonization process increases the density about .3-.4 which is expected due to the carbonization process.

2.3.4 Mechanical Behavior of Textile Carbon Fiber

Weibull distribution was assessed for the single filament data of the three fiber types and a commercial fiber. The Weibull distribution works very well with carbon fiber using the weakest link immediately fails approach. As the fiber length increases the chance of the weakest link increases and vice versa. This is automatically covered in Weibull where normal distribution assumes it doesn't matter where you choose the mean and standard deviation is the same. Using a 2 parameter Weibull distribution provides a strength and shape factor. The strength factor represents an equivalent to the mean in a normal distribution. The shape factor offers insight into the relative uniformity. In this study (Table 6) a commercial fiber was tested for a baseline of strength and shape factor giving 4849 MPa and 4.59 respectively. Textile carbon fiber's strength parameter is about half of the commercial fiber showing tensile strength limitation that needs to continue to improve. The scale parameter is also less than half of the commercial fiber showing

the uniformity issues within textile carbon fiber which could be due to the kidney bean shape of the fiber itself. Comparing the Weibull distributions shown in Figure 27 without the commercial fiber demonstrates that fiber A and C are nearly identical. This shows that the spin finish did not affect the overall single fiber tensile strength. Fiber B as mentioned earlier has a higher tenacity which intuitively influences the mechanical properties.

Assuming a normal distribution of the single carbon fibers of fiber A, B, and C shows an average failure stress of 2177, 2325, and 2164 MPa respectively shown in Table 7. A high standard deviation for each of the fiber sets could be attributed to the fiber being textile-based. Comparing the data of each fiber set shows that that fiber A and C are more similar with fiber B having slightly higher properties. This could be due to the processing conditions, but also could show that the higher tenacity influences the mechanical properties. The modulus data could be skewed since most tests didn't reach the required strain needed to calculate accurate data.

Comparing the single filament tensile strength data to the tow data in Table 8 demonstrates the information is very similar. The fiber tow properties are slightly higher with an emphasis on the failure stress and strain. Additional analysis would need to be completed, but one assumption could be that the fiber tow properties include the interfacial properties and stress transfer that would allow for the ability to exceed the single fiber properties. Analyzing the three fiber types in Table 8 shows the properties are all within 1.50% of their respective values. Based on these results we can determine that the spin finish and tenacity variation didn't provide an influence on the final tow properties.

To help with the analysis of the data, confidence intervals were determined. The distributions calculated from sample testing are substituted in the following format to construct confidence

intervals predicting the mean value of failure stress for all precursor populations at a 95% confidence level: $(\overline{y} - z_{\frac{\propto}{2}} * \frac{\sigma}{\sqrt{n}}, \overline{y} + z_{\frac{\propto}{2}} * \frac{\sigma}{\sqrt{n}})$. The confidence intervals, assuming a normal distribution, represent all estimates within two sigma limits of the mean value, meaning that they contain the inner 95% of the estimated population proportion. The confidence intervals for the mean values follow:

1. Fiber A (2353.718, 2659.51)
2. Fiber B (2372.903, 2566.282)
3. Fiber C (2463.277, 2549.03)

Following the calculation of the fiber type confidence intervals, the two-sample t test for difference of means is used to compare the distributions of each precursor using equation 4.

$$t = \frac{\overline{X_A} - \overline{X_B}}{\sqrt{\frac{S_A^2}{n_A} + \frac{S_B^2}{n_B}}} \quad (4)$$

We assume the test null hypothesis to be Ho: $\mu A = \mu B$ meaning that the mean failure stress of the samples being tested are equivalent. The alternative hypothesis proposed is Ha: $\mu A \neq \mu B$ meaning there exists a statistically significant difference in the failure stress mean values. The sample distributions can be used in the testing interchangeably. The t values and P-values calculated for all three comparison tests follow:

All t tests were conducting using the sample size (10) – 1 = 9 degrees of freedom.

1. Fiber B vs Fiber C
    a. T value: (-0.677504)
    b. P = 0.515122

2. Fiber C vs Fiber A
    a. T value: (-0.005683)
    b. P = 0.99559
3. Fiber B vs Fiber A
    a. T value: (-0.401107)
    b. P = 0.697968

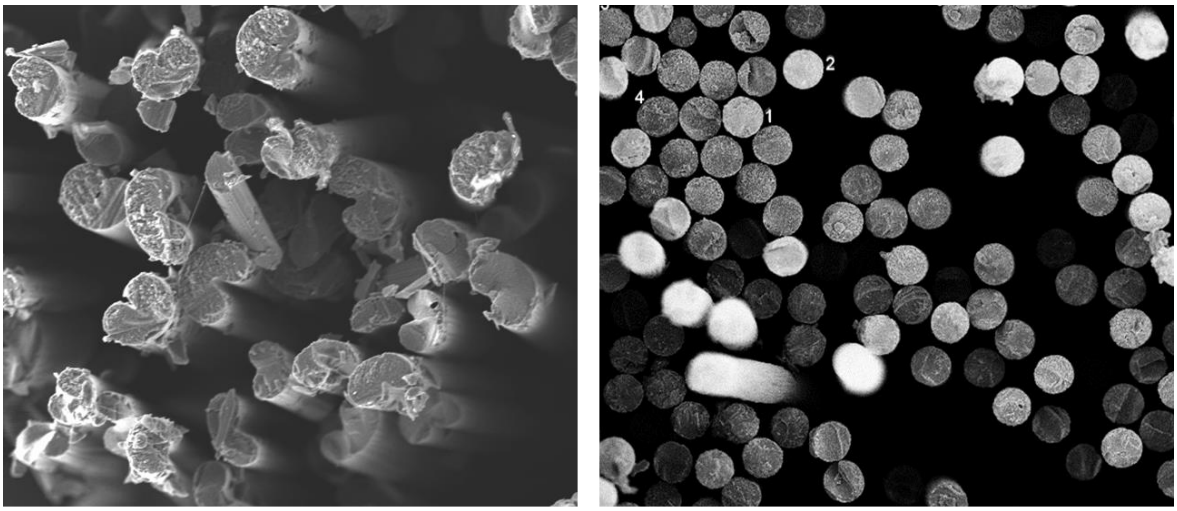
At an assumed α level of 0.05, all tests fail to reject the null hypothesis. There is not sufficient information to provide that there is a statistically significant difference in the mean values of failure stress between any of the 3 sample groups. The P values represent the probability of finding a more extreme t statistic for difference of mean failure stress. A high value of P, such as 0.99559 from the second test means that the probability of the difference in the means occurring in the circumstances of the null hypothesis is almost 1 of 1. Further testing needs to be conducted on various levels of spin finish and tenacity to determine effect and significant outcomes.

2.4 Conclusions

Three textile precursors were received and converted to carbon fiber using a conventional conversion process. The precursor and oxidized PAN fiber were characterized by thermogravimetric analysis (TGA), differential scanning calorimetry (DSC), X-ray diffraction, and Fourier Transform Infrared spectroscopy (FT-IR). Additionally, single filament and infused tow testing were performed on the carbon fibers of each fiber type. The FT-IR spectra for the precursor and OPF material showed consistent peaks with literature and between each fiber type showing little difference. The TGA analysis of the precursor and OPF material demonstrated

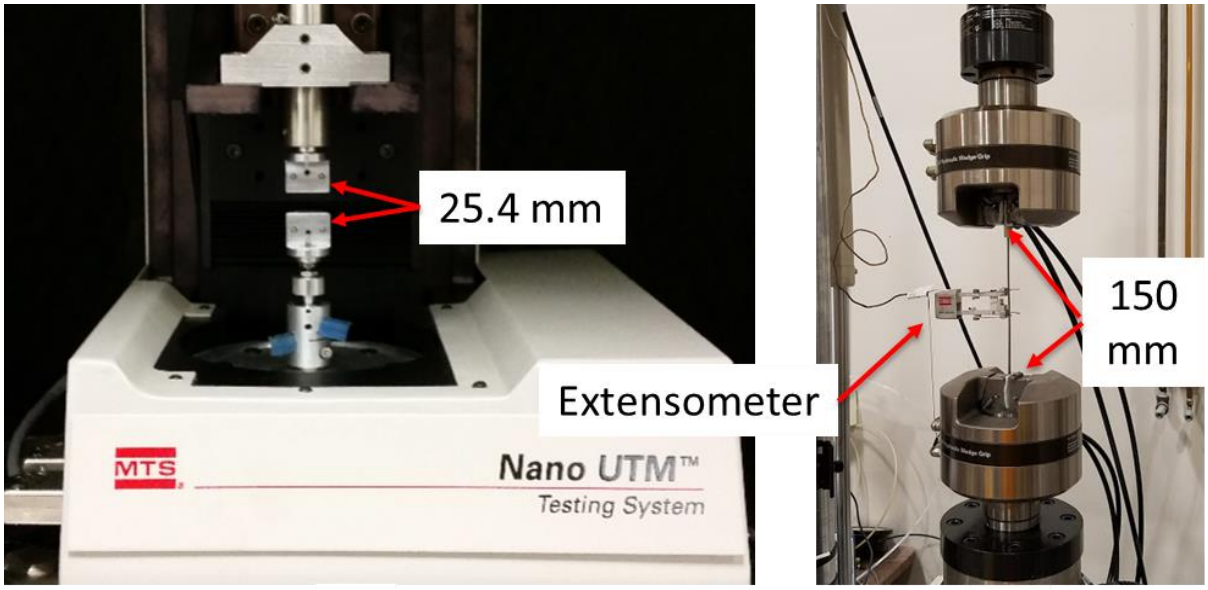
almost identical mass loss trends between fiber A, B, and C. DSC analysis was completed for the precursor and OPF material as well. This showed very similar onset temperatures, peak temperatures, and the enthalpies calculated. Ratios were calculated between the precursor and OPF for fiber A, B, and C which were 64%, 79%, and 78% respectively. This could be a representation of the oxidation and the potential of the fiber not being fully oxidized before entering the subsequent process in the conversion. X-ray diffraction demonstrated the atomic structure of the three fiber types were practically identical regardless of the spin finish or tenacity. The data from the single fiber testing showed that the spin finish had no effect on the final properties of the carbon fiber, but the tenacity did have a slight increase in properties. Tow testing was completed on the fiber types, and we found the tightest distribution was with Fiber C which seemed to perform better within the measurement error. In general, we didn't see big changes which indicate this process is more flexible in terms of the what precursor that one uses during oxidation and carbonization process. The initial analysis results indicate that the spin finish didn't influence the overall thermal and mechanical properties despite potential processing variation. Tenacity did cause a slight effect on the single fiber properties, but it can't be ruled out that the processing differences could've contributed to this. In general, the conclusions of low cost carbon fibers show more deviation in property variation, with modulus looking consistent but the tensile strength much lower than commercial.

2.5 Appendix



a) b)

Figure 15 - SEM comparing the a) kidney bean cross-section shape of the textile carbon fiber b) circular cross-section of commercial carbon fiber



a) b)

Figure 16 - Example tensile testing setup of a) single fiber testing using the Nano UTM and b) infused tow testing using the MTS test system

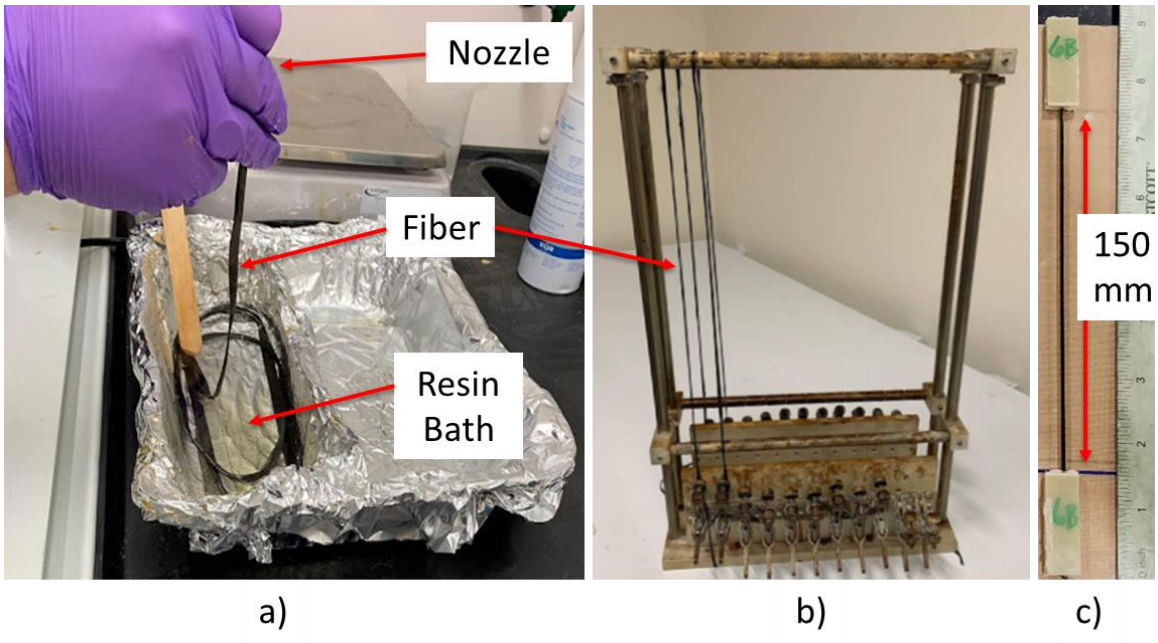


Figure 17 - Example procedure of a) fiber tow resin infusion b) rack attachment to keep taut c) final tabbed strand

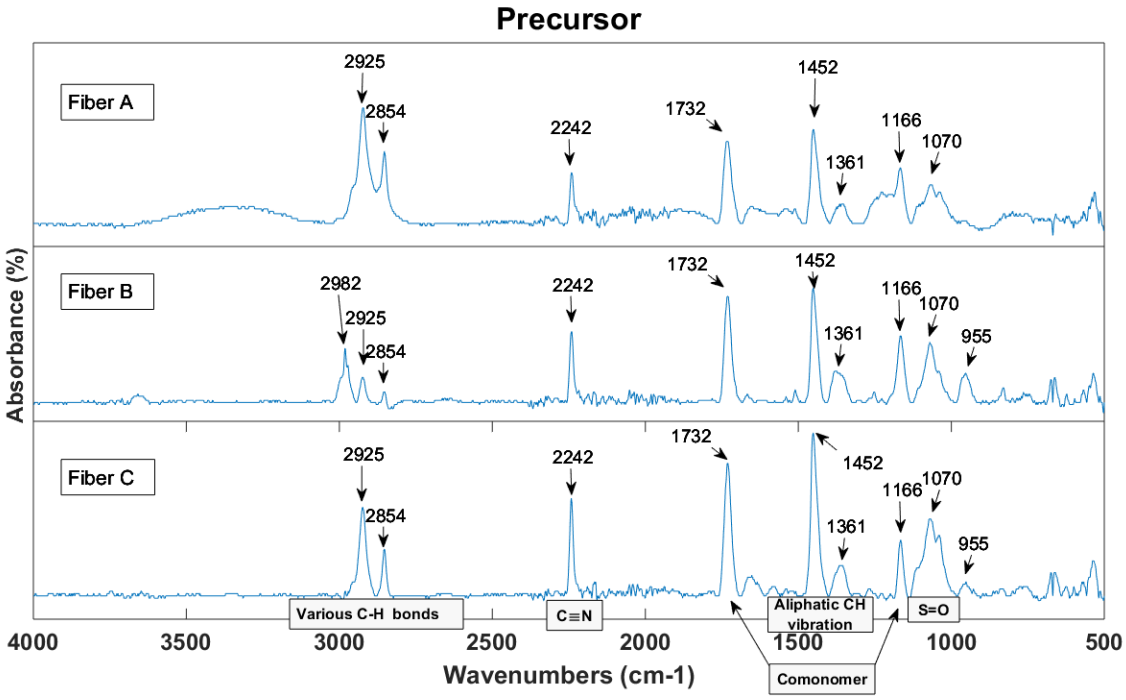


Figure 18 - FT-IR spectra of textile PAN precursors A, B, and C showing surface functional groups before the oxidation process.

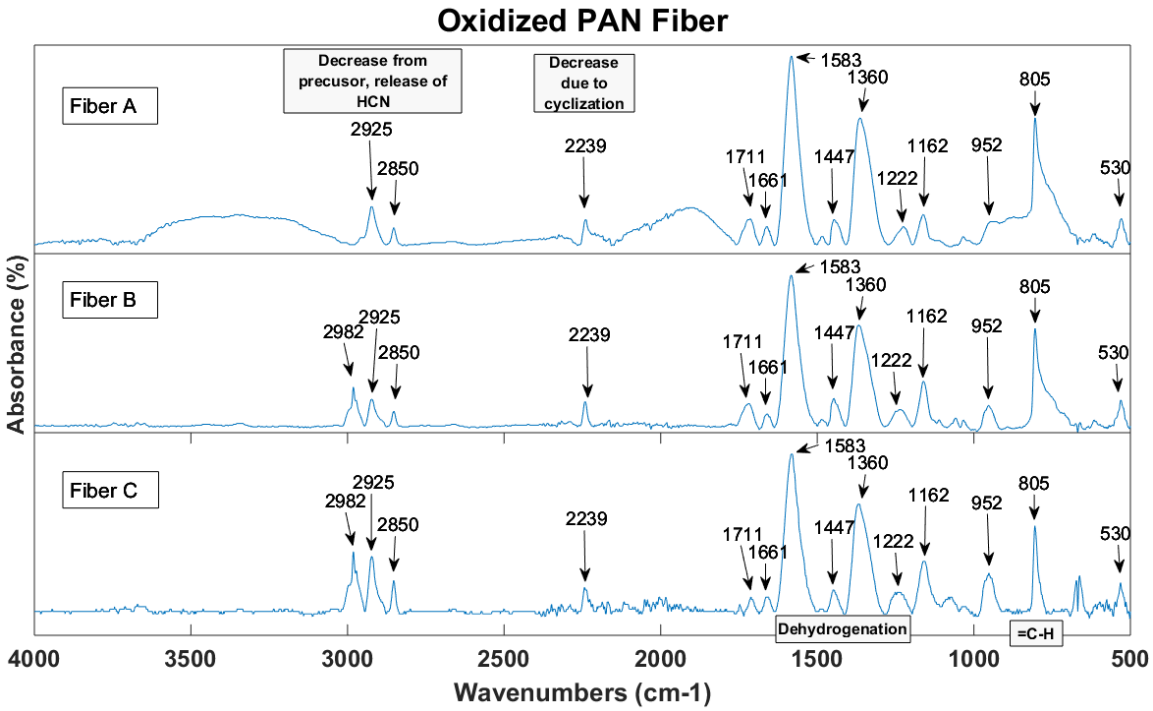


Figure 19 - FT-IR spectra of the textile PAN fibers A, B, and C after oxidation demonstrating surface functional groups increase/decrease from the precursor.

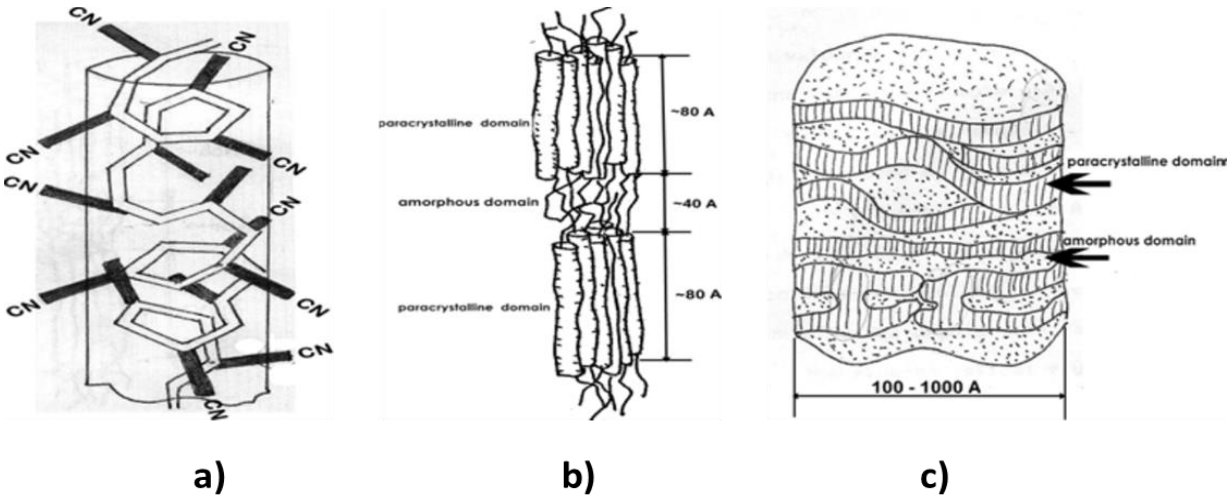


Figure 20 - Schematic illustration of the PAN structural levels: a) macromolecule helical structure; b) macromolecular orientation; c) fibril.Note: Reprinted from Violeta Florina Anghelina et al. Structural analysis of PAN fiber by X-ray diffraction, Journal of Science and Arts 1(12) (2010) 89-94 [50]

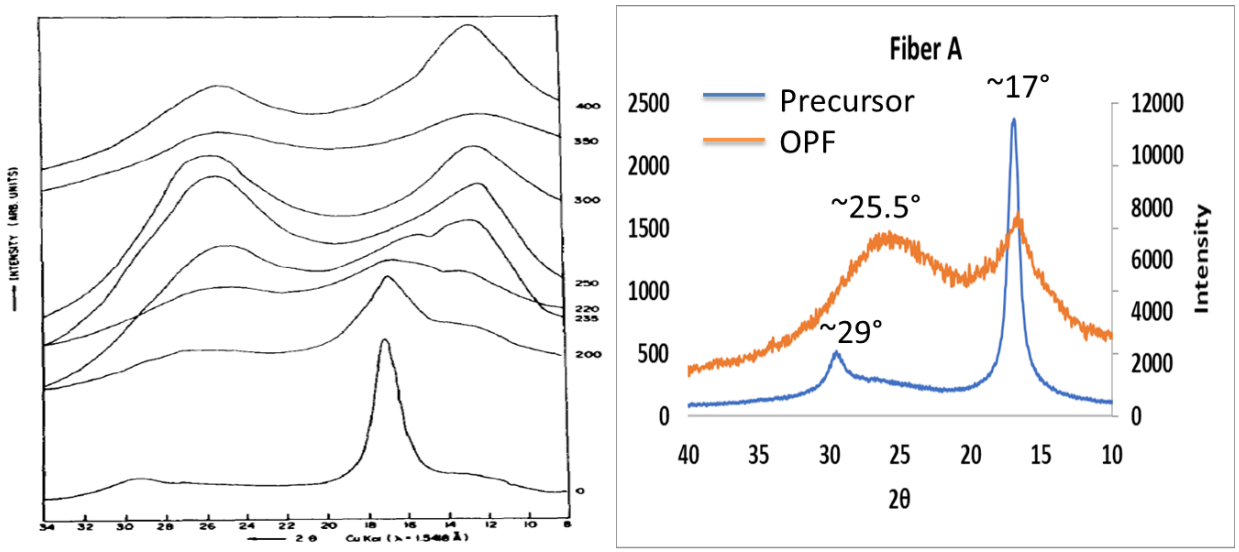


Figure 21 - X-ray diffraction patterns for a) commercial PAN pure and oxidized b) textile PAN pure and oxidized Note a) is a reprint from R. B. Mathur "Structure of thermally stabilized PAN fibers", Carbon 29(7) (1991) 1059-1061 [49]

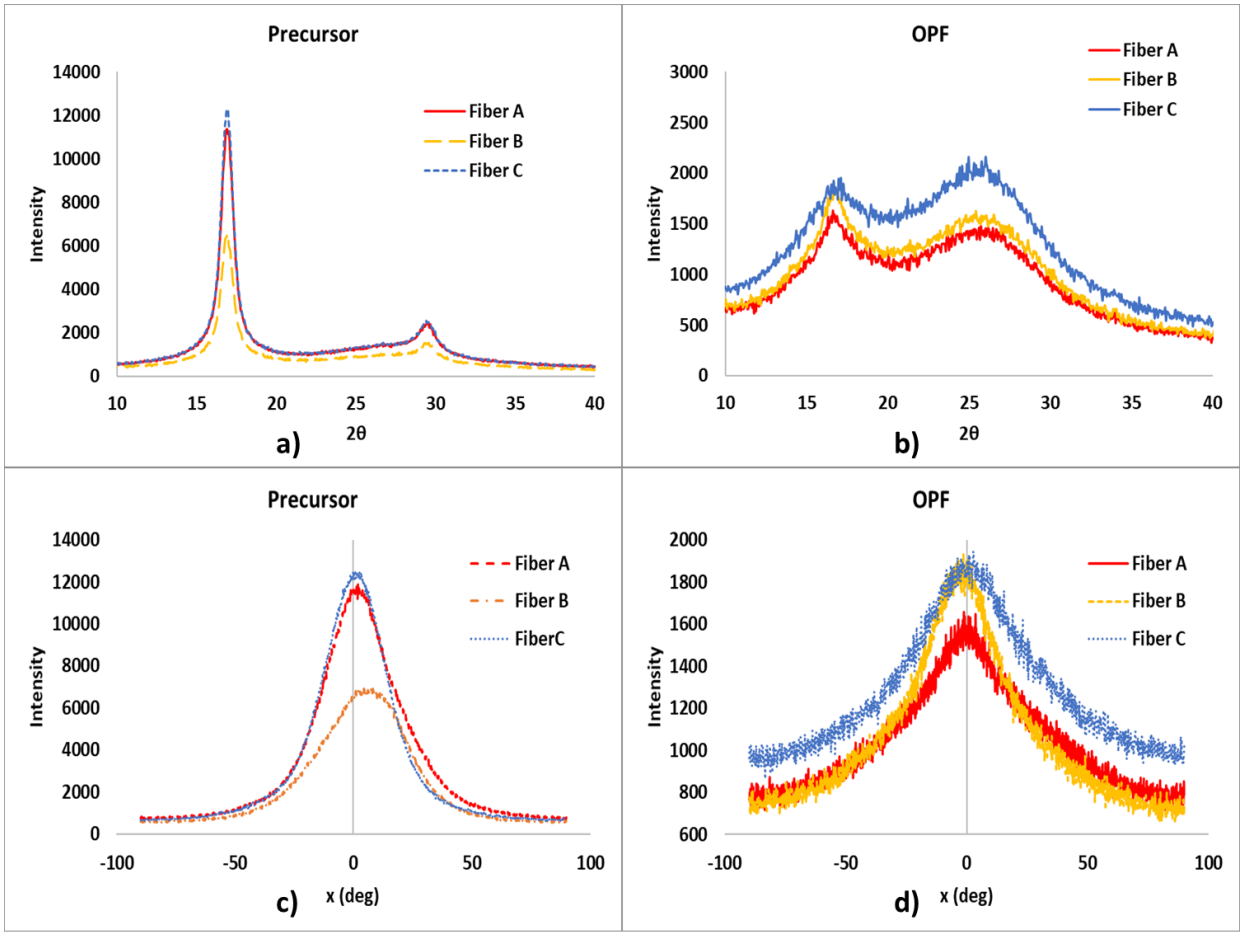


Figure 22 - Comparison of x-ray diffraction pattern for the 2θ a) precursor fiber A, B, and C b) OPF fiber A, B, and C; and orientation comparison of c) precursor fiber A, B, and C and d) OPF fiber A, B, and C.

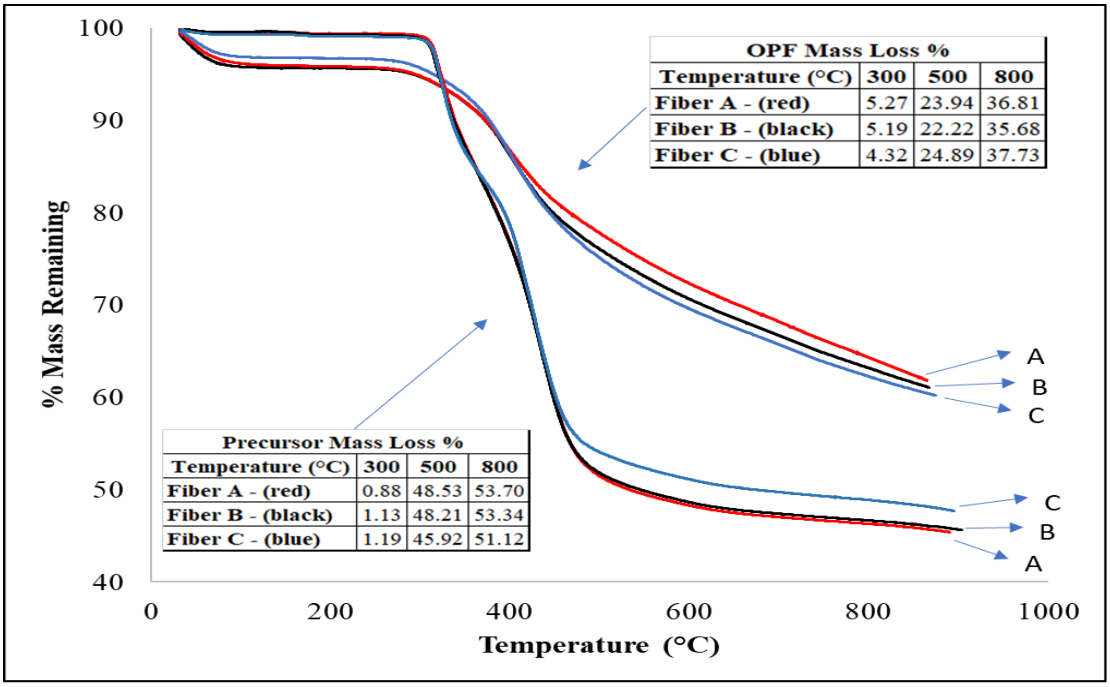


Figure 23 - TGA thermogram (nitrogen atmosphere) of the three precursors and oxidized PAN fibers showing mass loss prior to carbonization ad showing good agreement to the DSC thermal information.

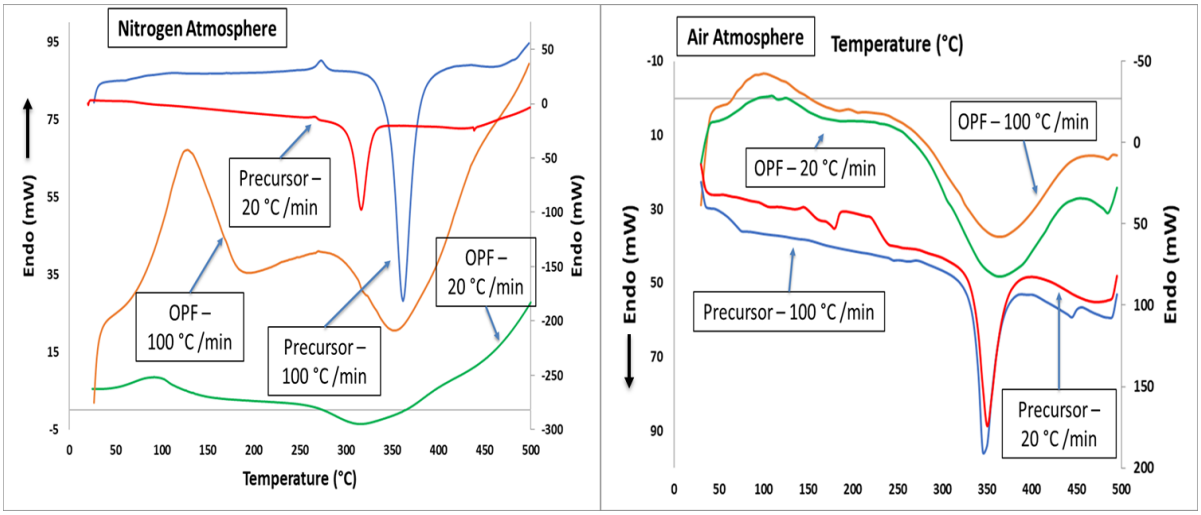


Figure 24 - DSC analysis comparing a fast and slow heating rate and the effect the environment has on the thermal analysis using nitrogen (inert) atmosphere and air atmosphere.

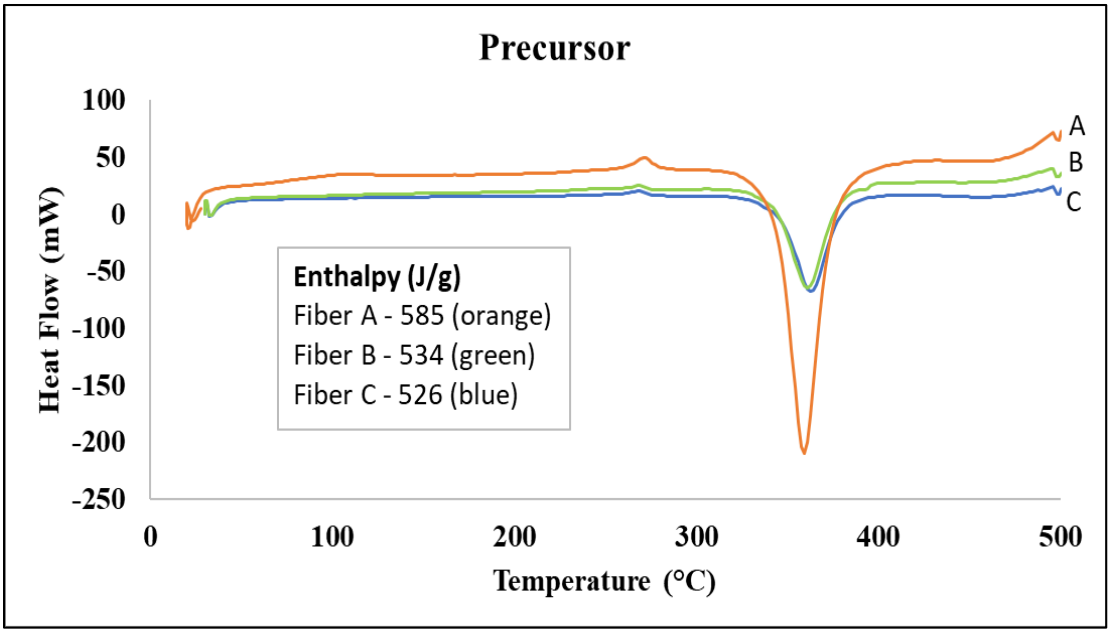


Figure 25 - DSC thermogram of the precursor for fiber A, B, and C showing similar peak temperatures and measured enthalpies.

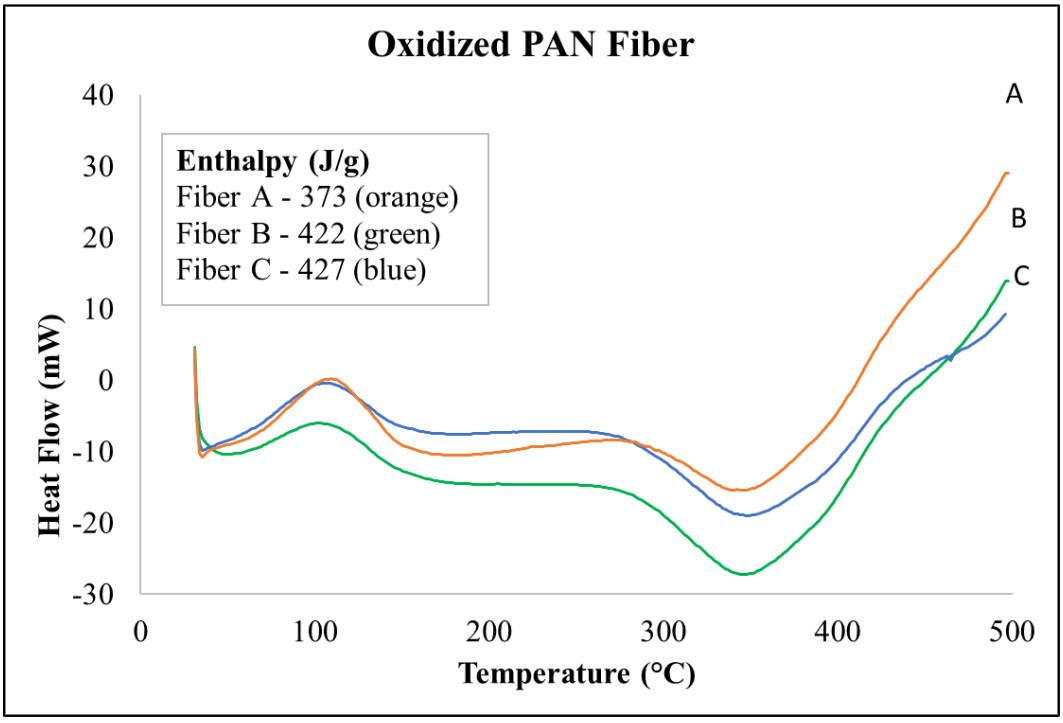


Figure 26 - DSC thermogram of the oxidized PAN fiber A, B, and C demonstrating similar enthalpy values for each fiber and a peak at `100 °C indicating moisture evaporation.

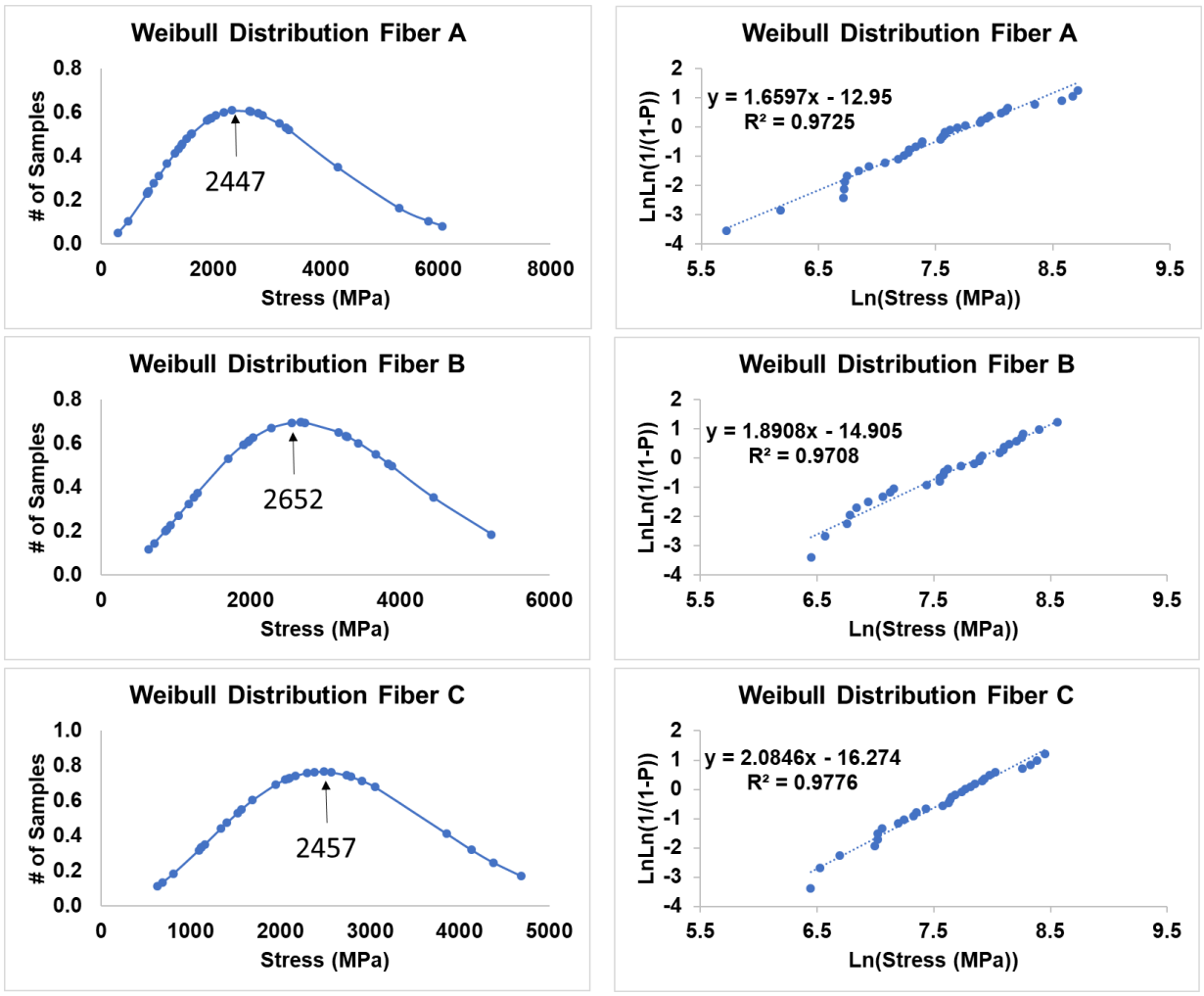


Figure 27 - Weibull distribution of single filament data for fiber A, B, and C showing consistent strength and scale parameters. The low scale parameters (1.66, 1.89, 2.08) demonstrate high strength variation.

Table 4 X-ray diffraction peak locations, full width half max (FWHM), d-spacing, and stack height for Fiber A, B, and C precursor and OPF.

Precursor									
	Peak 1	Peak 2	FWHM	FWHM	$d_{(100)}$	$d_{(110)}$	Lc	Lc	Chi Peak 1 FWHM
	(2θ)	(2θ)	(°)	(°)	(Å)	(Å)	(Å)	(Å)	(°)
Fiber A	16.93	29.50	0.929	1.361	0.939	0.943	1.492	1.042	37.539
Fiber B	16.91	29.51	0.941	1.202	0.935	0.945	1.473	1.180	42.774
Fiber C	16.92	29.49	0.918	1.325	0.937	0.939	1.510	1.070	32.659
OPF									
	Peak 1	Peak 2	FWHM	FWHM	$d_{(100)}$	$d_{(002)}$	Lc	Lc	Chi Peak 1 FWHM
	(2θ)	(2θ)	(°)	(°)	(Å)	(Å)	(Å)	(Å)	(°)
Fiber A	16.73	25.73	4.376	8.384	0.883	2.615	0.317	0.168	59.562
Fiber B	16.56	25.50	3.893	8.621	0.847	4.231	0.356	0.163	56.407
Fiber C	16.74	25.73	6.196	8.957	0.886	2.619	0.224	0.157	47.303

Table 5 DSC thermal characterization analysis data demonstrating similarity of Fiber A, B, and C

Material	Density	Enthalpy	Onset	Peak
	g/cm^3	J/g	°C	°C
Precursor Fiber A	1.2236	586	344	359
Precursor Fiber B	1.2057	535	343	361
Precursor Fiber C	1.2080	526	346	363
OPF Fiber A	1.3878	377	281	354
OPF Fiber B	1.3733	424	274	352
OPF Fiber C	1.3938	409	273	351

Table 6 Single filament Weibull strength and shape parameters

	Weibull Strength Parameter	Weibull Shape Parameter
	MPa	
Commercial Fiber	4849	4.59
Fiber A	2447	1.66
Fiber B	2652	1.89
Fiber C	2457	2.08

Table 7 Average single filament mechanical results using normal distribution

	Failure Stress	St. Dev.	Failure Strain	St. Dev.	Modulus	St. Dev.
	MPa	MPa	mm/mm	mm/mm	GPa	GPa
Commercial Fiber	4434	1045	1.85%	0.40%	260	21
Fiber A	2177	1443	0.65%	0.42%	350	167
Fiber B	2325	1221	0.68%	0.49%	378	185
Fiber C	2164	1093	0.66%	0.38%	340	131

Table 8 Infused tow mechanical properties

	Density	Failure Stress	St. Dev.	Failure Strain	St. Dev.	Modulus	St. Dev.
	g/cm^3	MPa	MPa	mm/mm	mm/mm	GPa	GPa
Fiber A	1.7486	2507	260	0.99%	0.08%	257	12
Fiber B	1.7648	2470	164	0.97%	0.05%	265	12
Fiber C	1.7738	2506	73	0.97%	0.04%	263	8

CONCLUSION

1. ASTM D4018-11 was used to prepare the impregnated fiber tow samples using the suggested automated and manual methods. There was about a 6% increase in ultimate failure stress from the automated method to the manual method.
2. Proposed a new parameter limit stress which use the single fiber inherent properties to show when the sample deviates from nonlinearity. This could be potentially used as a quick way to help determine interfacial behavior between fibers and different matrix systems.
3. FT-IR, XRD, DSC, and TGA analysis of the three precursors and OPFs showed little variation despite the differences of spin finish and tenacity.
4. Single fiber and infused tow testing indicates that there is more deviation in mechanical properties than commercial fiber, but the role of spin finish and tenacity has minimal effect demonstrating the flexibility of low-cost textile PAN precursor.

REFERENCES

1-78

[1] D. Church, A revolution in low-cost carbon fiber production, Reinforced Plastics 62(1) (2018) 35-37.

[2] S. Phrukkanon, M.F. Burrow, M.J. Tyas, The influence of cross-sectional shape and surface area on the microtensile bond test, Dental Materials (14) (1998) 212-221.

[3] R.B. Durairaj, G. Mageshwaran, V. Sriram, Investigation on Mechanical Properties of Glass and Carbon Fiber Reinforced With Polyester Resin Composite, International Journal of ChemTech Research 9(06) (2016) 417-423.

[4] I.M. Daniel, O. Ishai, Engineering Mechanics of Composite Materials. Second Edition, Oxford University Press, Inc., New York, 2006.

[5] A. International, Standard Test Methods for Properties of Continuous Filament Carbon and Graphite Fiber Tows, 2011, p. 7.

[6] F. Tanaka, T. Okabe, H. Okuda, I.A. Kinloch, R.J. Young, Factors controlling the strength of carbon fibres in tension, Composites Part A: Applied Science and Manufacturing 57 (2014) 88-94.

[7] T. Tagawa, T. Miyata, Size effect on tenstile strength of carbon fibers, Materials Science & Engineering A A238 (1997) 336-342.

[8] K. Dong, J. Zhang, M. Cao, M. Wang, B. Gu, B. Sun, A mesoscale study of thermal expansion behaviors of epoxy resin and carbon fiber/epoxy unidirectional composites based on periodic temperature and displacement boundary conditions, Polymer Testing 55 (2016) 44-60.

[9] T.-W. Chou, L. Gao, E.T. Thostenson, Z. Zhang, J.-H. Byun, An assessment of the science and technology of carbon nanotube-based fibers and composites, Composites Science and Technology 70(1) (2010) 1-19.

[10] D.W.P. Jr., Development and Validation of a Dry Fiber Bundle Test Method, Chemical Engineering, Montana State Univeristy-Bozeman, 2000, p. 182.

[11] D. Loidl, H. Peterlik, O. Paris, M. Muller, M. Burghammer, C. Riekel, Structure and mechanical properties of carbon fibres: a review of recent microbeam diffraction studies with synchrotron radiation, J Synchrotron Radiat 12(Pt 6) (2005) 758-64.

[12] M.E. Kant, Single Fiber Mechanical Properties Using Nano-Tensile Testing and Carbon Fiber Structure-Property Relationship, Mechanical Engineering, University of Tennessee, 2014.

[13] M. Kant, D. Penumadu, Dynamic mechanical characterization for nonlinear behavior of single carbon fibers, Composites Part A: Applied Science and Manufacturing 66 (2014) 201-208.

[14] J.B. Hurst, W.S. Hong, M.L. Gambone, J.R. Porter, ASTM Single Fiber Room Temperature Test Standard Development, (78668) (1998) V005T13A017.

[15] J. Charles P. Beetz, A Self-Consistent Weibull Analysis of Carbon Fibre Strength Distributions, Fibre Science and Technology (16) (1982) 81-94.

[16] N. Meek, D. Penumadu, O. Hosseinaei, D. Harper, S. Young, T. Rials, Synthesis and characterization of lignin carbon fiber and composites, Composites Science and Technology 137 (2016) 60-68.

[17] A. Kelly, W.R. Tyson, Tensile properties of fibre-reinforced metals: Copper/tungsten and copper/molybdenum, Journal of the Mechanics and Physics of Solids 13 (1965) 329-350.

[18] S. Feih, K. Wonsyld, D. Minzari, P. Westermann, H. Lilholt, Establishing a Testing Procedure for the Single Fiber Fragmentation Test, in: Risø-R-1483(EN) (Ed.) 2004.

[19] L.T. Drzal, M. Madhukar, Fibre-matrix adhesion and its relationship to composite mechanical properties, Journal of Materials Science 28 (1993) 569-610.

[20] A. Siriruk, D. Penumadu, Y. Jack Weitsman, Effect of sea environment on interfacial delamination behavior of polymeric sandwich structures, Composites Science and Technology 69(6) (2009) 821-828.

[21] F. Gnädinger, P. Middendorf, B. Fox, Interfacial shear strength studies of experimental carbon fibres, novel thermosetting polyurethane and epoxy matrices and bespoke sizing agents, Composites Science and Technology 133 (2016) 104-110.

[22] S.-J. Park, G.-Y. Heo, Precursors and Manufacturing of Carbon Fibers, Carbon Fibers2015, pp. 31-66.

[23] H.D. Cochran, Analysis of Carbon Fiber Characterization Techniques, Aerospace Engineering, The University of Tennessee, Knoxville, http://trace.tennessee.edu/utk_gradthes/3649, 2008, p. 148.

[24] H.H. Shin, Low Cost Manufacturing Process of Carbon Fiber and Composites, 2011.

[25] G.S. BHAT, F.L. COOK, A.S. ABHIRAMAN, J. L. H. PEEBLES, New Aspects in the Stabilization of Acrylic Fibers for Carbon Fibers, Carbon 28 (1990) 377-385.

[26] S. Deng, L. Ye, Y.-W. Mai, Infuence of fibre cross-sectional aspect ratio on mechanical properties of glass fibre/epoxy composites I. Tensile and flexure behaviour, Composites Science and Technology (1998) 1331-1339.

[27] D.K. Singh, Computational Modeling and Surface Characterization of Interface in Polymer Composites by Atomic Force Microscopy, Material Science and Engineering, The University of Alabama At Birmingham, 2015, p. 89.

[28] Z. Wangxi, L. Jie, W. Gang, Evolution of structure and properties of PAN precursors during their conversion to carbon fibers, Carbon 41(14) (2003) 2805-2812.

[29] T. Mikolajczyk, S. Rabiej, G. Szparaga, M. Boguń, A. Fraczek-Szczypta, S. Błażewicz, Strength Properties of Polyacrylonitrile (PAN) Fibres Modified with Carbon Nanotubes with Respect to Their Porous and Supramolecular Structure, Fibres and Textiles 17 (2009) 13-20.

[30] L. Kong, H. Liu, W. Cao, L. Xu, PAN fiber diameter effect on the structure of PAN-based carbon fibers, Fibers and Polymers 15(12) (2015) 2480-2488.

[31] A.K. GUPTA, A.K. MAITI, Effect of Heat Treatment on the Structure and Mechanical Properties of Polyacrylonitrile Fibers, Applied Polymer Science 27 (1982) 2409-2416.

[32] H. Ge, H. Liu, J. Chen, C. Wang, The microstructure of polyacrylonitrile-stabilized fibers, Journal of Applied Polymer Science 113(4) (2009) 2413-2417.

[33] P. Bajaj, A.K. Roopanwal, Thermal Stabilization of Acrylic Precursors for the Production of Carbon Fibers: An Overview, Journal of Macromolecular Science, Part C: Polymer Reviews 37(1) (1997) 97-147.

[34] JIN-SHYTSAI, H.-N. HSU, Determination of the aromatization index for oxidized polyacrylonitrile fibre by the differential scanning calorimetry method, Materials Science Letters 11 (1992) 1403-1405.

[35] J.-S. TSAI, C.-H. LIN, The Effect of Molecular Weight on the Cross Section and Properties of Polyacrylonitrile Precursor and Resulting Carbon Fiber, Applied Polymer Science 42 (1991) 3045-3050.

[36] E. FITZER, W. FROHS, M. HEINE, Optimization of Stabilization and Carbonization Treatment of PAN Fibres and Structural Characterization of the Resulting Carbon Fibres, Carbon 4 (1986) 387-395.

[37] R.F. Ribeiro, L.C. Pardini, N.P. Alves, C.A.R. Brito Júnior, Thermal Stabilization study of polyacrylonitrile fiber obtained by extrusion, Polímeros 25(6) (2015) 523-530.

[38] S. Lee, J. Kim, B.-C. Ku, J. Kim, H.-I. Joh, Structural Evolution of Polyacrylonitrile Fibers in Stabilization and Carbonization, Advances in Chemical Engineering and Science 02(02) (2012) 275-282.

[39] J. Mittal, O.P. Bahl, R.B. Mathur, N.K. Sandle, IR studies of PAN fibres thermally stabilized at elevated temperatures, Carbon 32(6) (1994) 1133-1136.

[40] U.A. Sayed, A. Shirsat, A. Shinde, A. Lahariya, Effect of Wet-Spinning Parameters and Spin-Finish Application on Production of Polyacrylonitrile Precursor for Carbon Fibre Production, International Journal of Advanced Science and Engineering 3(2) (2016) 286-288.

[41] W. Postman, Spin Finishes Explained, Textile Research Journal (1980) 444-452.

[42] E.A. Morris, M.C. Weisenberger, Solution Spinning of PAN-Based Polymers for Carbon Fiber Precursors, in: N.a. Hoffman (Ed.) Polymer Precursor-Derived Carbon ACS Symposium Series, American Chemical Society, Washington, DC, 2014, pp. 190-213.

[43] J.-S. TSAI, C.-H. LIN, Effect of Comonomer Composition on the properties of Polyacrylonitrile Precursor and Resulting Carbon Fiber, Journal of Applied Polymer Science 43 (1991) 679-685.

[44] Z. Xu, J. Li, X. Wu, Y. Huang, L. Chen, G. Zhang, Effect of kidney-type and circular cross sections on carbon fiber surface and composite interface, Composites Part A: Applied Science and Manufacturing 39(2) (2008) 301-307.

[45] I.M. Alarifi, A. Alharbi, W.S. Khan, A. Swindle, R. Asmatulu, Thermal, Electrical and Surface Hydrophobic Properties of Electrospun Polyacrylonitrile Nanofibers for Structural Health Monitoring, Materials (Basel) 8(10) (2015) 7017-7031.

[46] R.E. Farsani, S. Raissi, A. Shokuhfar, A. Sedghi, FT-IR Study of Stabilized PAN Fibers for Fabrication of Carbon Fibers, International Journal of Mechanical and Mechatronics Engineering 3(2) (2009).

[47] I. SHIMADA, T. TAKAHAGI, M. FUKUHARA, K. MORITA, A. ISHITANI, FT-IR Study of the Stabilization Reaction of Polyacrylonitrile in the Production of Carbon Fibers, Polymer Science Part A: Polymer Chemistry 24 (1986) 1989-1995.

[48] G.T. Sivy, M.M. Coleman, Fourier Transform IR Studies of the Degradation of Polyacrylonitrile Copolymers—II: Acrylonitrile/Methacrylic Acid Copolymers, Carbon 19 (1980) 127-131.

[49] R.B. Mathur, O.P. Bahl, J. Mittal, K.C. Nagpal, Structure of thermally stabilized PAN fibers, Carbon 29(7) (1991) 1059-1061.

[50] V.F. ANGHELINA, I.V. POPESCU, A. GABA, I.N. POPESCU, V. DESPA, D. UNGUREANU, Structural analysis of PAN fiber by X-ray diffraction, Journal of Science and Arts 1(12) (2010) 89-94.

[51] H. Ahmadian, B. Liang, S. Soghrati, An integrated computational framework for simulating the failure response of carbon fiber reinforced polymer composites, Computational Mechanics 60(6) (2017) 1033-1055.

[52] W.D. Bascom, R.M. Jensen, Stress Transfer in Single Fiber/ Resin Tensile Tests, The Journal of Adhesion 19(3-4) (2006) 219-239.

[53] H.G. Chae, Y.H. Choi, M.L. Minus, S. Kumar, Carbon nanotube reinforced small diameter polyacrylonitrile based carbon fiber, Composites Science and Technology 69(3-4) (2009) 406-413.

[54] D. Cohen, K.A. Lowe, The Influence of Epoxy Matrix Properties on Delivered Fiber Strength in Filament Wond Composite Pressure Vessels, Reinforced Plastics and Composites 10 (1991) 20.

[55] J. Crabtree, D. Penumadu, S. Young, Tensile Properties of Carbon Fiber: Single Filament Vs Tow Based Testing, American Society for Composites: Thirty-Second Technical Conference, DEStech Publications, Inc., Purdue University, West Lafayette, Indiana, October 23-25, 2017. Lancaster, PA, USA, 2017, p. 11.

[56] P.D. H. E. Daniels, The statistical theory of the strength of bundles of threads. I, Proceedings of the Royal Society of London. Series A. Mathematical and Physical Sciences 183 (1945) 405-435.

[57] H.M. Hsaio, I.M. Daniel, Elastic properties of composites with fiber waviness, Composites Part A: Applied Science and Manufacturing (1996) 931-941.

[58] X. Huang, Fabrication and Properties of Carbon Fibers, Materials 2(4) (2009) 2369-2403.

[59] J.D.H. Hughes, The Carbon Fibre-Epoxy Interface - A Review, Composites Science and Technology 41 (1991) 13-45.

[60] W. Jiao, W. Liu, F. Yang, L. Jiang, W. Jiao, R. Wang, Improving the interfacial property of carbon fiber/vinyl ester resin composite by grafting modification of sizing agent on carbon fiber surface, Journal of Materials Science 52(24) (2017) 13812-13828.

[61] Y.M. K. Morita, A. Ishitani, K. Murayama, T. Ono, A. Nakajima, Characterization of Commercially Available PAN (Polyacrylonitrile)-based Carbon Fibers, Pure and Applied Chemistry 58(3) (1986) 455-468.

[62] A.T. Kalashnik, T.N. Smirnova, O.P. Chernova, V.V. Kozlov, Properties and structure of polyacrylonitrile fibers, Polymer Science Series A 52(11) (2010) 1233-1238.

[63] M. Kant, D. Penumadu, Fracture behavior of individual carbon fibers in tension using nano-fabricated notches, Composites Science and Technology 89 (2013) 83-88.

[64] B. Lee, K.H. Leong, I. Herszberg, Effect of Weaving on the Tensile Properties of Carbon Fibre Tows and Woven Composites, Journal of Reinforced Plastics and Composites 20(8) (2001) 652-670.

[65] W.I. Lee, G.S. Springer, A Model of the Manufacturing Process of Thermoplastic Matrix Composites, Composite Materials 21 (1987) 39.

[66] T.C. Lim, Simplified Transverse Young's Modulus of Aligned Ribbon-Reinforced Composites by the Mechanics-of-Materials Approach, Reinforced Plastics and Composites 22 (2003).

[67] J. LIU, P.H. WANG, R.Y. LI, Continuous Carbonization of Polyacrylonitrile-Based Oxidized Fibers: Aspects on Mechanical Properties and Morphological Structure, Applied Polymer Science 52 (1994) 945-950.

[68] M.-y. Lv, H.-y. Ge, J. Chen, Study on the chemical structure and skin-core structure of polyacrylonitrile-based fibers during stabilization, Journal of Polymer Research 16(5) (2008) 513-517.

[69] A. Maier, R. Schledjewski, Study on parameters affecting the mechanical properties of dry fiber bundles during continuous composite manufacturing processes, IOP Conference Series: Materials Science and Engineering 139 (2016).

[70] B. Pan, L. Tian, Advanced video extensometer for non-contact, real-time, high-accuracy strain measurement, Opt Express 24(17) (2016) 19082-93.

[71] D. Penumadu, J.D. Crabtree, M.E. Kant, S.A. Young, N.K. Meek, Characterization Inspired Manufacturing of Carbon Fiber Composites Considering Multiscale Response, American Society for Composites, Williamsburg Lodge Hotel, 2016.

[72] M.S.A. Rahaman, A.F. Ismail, A. Mustafa, A review of heat treatment on polyacrylonitrile fiber, Polymer Degradation and Stability 92(8) (2007) 1421-1432.

[73] M. Sharma, S. Gao, E. Mäder, H. Sharma, L.Y. Wei, J. Bijwe, Carbon fiber surfaces and composite interphases, Composites Science and Technology 102 (2014) 35-50.

[74] M. Shioya, A. Takaku, Estimation of Fibre and Interfacial Shear Strength By Using A Single-Fibre Composite, Composites Science and Technology 55 (1995) 33-39.

[75] S. Tiwari, M. Sharma, S. Panier, B. Mutel, P. Mitschang, J. Bijwe, Influence of cold remote nitrogen oxygen plasma treatment on carbon fabric and its composites with specialty polymers, Journal of Materials Science 46(4) (2010) 964-974.

[76] E. Toptaş, N. Akkuş, Damage detection of carbon fibers in filament winding machines using an electrical resistance method, The International Journal of Advanced Manufacturing Technology 93(1-4) (2017) 671-679.

[77] H.D. Wagner, A. Eitan, Stress Concentration Factors in Two-Dimensional Composites: Effects of Material and Geometrical Parameters, Composites Science and Technology 46 (1992) 353-362.

[78] R.J. Zaldivar, G.S. Rellick, J.M. Yang, Fiber strength utilization in carbon/carbon composites, Journal of Materials Research 8(03) (2011) 501-511.

VITA

Joshua David Crabtree was born in Knoxville, Tennessee on February 6, 1992. Josh graduated from Midway High School in 2010 after which he attended Roane State Community College. After receiving his Associate degree in Pre-Engineering, Josh transferred to Tennessee Technological University to finish his Bachelor's in Chemical Engineering. After graduation in May 2015 he worked full-time as an intern at the Carbon Fiber Technology Facility with ORAU. January 2016 Josh continued his education by pursuing a Master's in Engineering Science at the University of Tennessee doing research with carbon fiber composite materials in collaboration with the CFTF. He obtained his degree in May 2019. During his graduate program, leaning on his faith, Josh announced his call to preach the gospel at his home church Salem Baptist Church in Ten Mile, TN on September 25, 2016. After graduation Josh will continue to work and preach following direction from the Lord on where to go.